

Volume-entangled exact eigenstates in the PXP and related models in any dimension

Andrew N. Ivanov and Olexei I. Motrunich

Department of Physics and Institute for Quantum Information and Matter,
California Institute of Technology, Pasadena, California 91125, USA

(Dated: April 15, 2024)

In this work, we report first exact volume-entangled Einstein-Podolsky-Rosen (EPR) type scar states hosted by PXP and related Hamiltonians corresponding to various geometric configurations of Rydberg-blockaded atom systems, including the most extensively studied ones such as the chain with periodic boundary conditions (PBC) and square lattice. We start by introducing a new zero-energy eigenstate of the PBC chain and proceed by generalizing it to a wide variety of geometries and Hamiltonians. We point out the experimental relevance of such states by providing a concrete and feasible protocol for their preparation on near-term Rydberg quantum devices, which relies only on strictly local measurements and evolution under native Hamiltonians. We also demonstrate the utility of these states for the study of quantum dynamics by describing a simple protocol for measuring infinite-temperature out-of-time-order correlator (OTOC) functions.

Introduction.— The observation of unusually slow thermalization and unexpected many-body revivals during a quench from a Néel-type state in the pioneering Rydberg atom experiment [1] ignited interest in the so-called PXP model [2], which is an idealized description of Rydberg atomic systems in the nearest-neighbor blockade regime. The attribution of this atypical dynamics to the presence of special “scar” eigenstates weakly violating the eigenstate thermalization hypothesis (ETH) in the spectrum of the one-dimensional PXP Hamiltonian [3, 4] opened the field of quantum many-body scars [5–7]. Various perspectives on the mechanisms underlying these states have been put forth [3, 4, 8–17], yet no comprehensive theory is currently available (for reviews see [18–22]). Despite their apparent simplicity, PXP Hamiltonians, being non-integrable and chaotic based on the level statistics, typically elude analytical treatments, which is evident from the scarcity of exact results. For example, only two exact zero energy eigenstates related by translation are currently known for the PXP chain with PBC [9]; exponentially many states with valence bond solid orders have been found in two-dimensional PXP models [23, 24]. All currently known exact eigenstates exhibit area law scaling of entanglement.

Eigenstate of the PXP chain.— Consider a state on a spin-1/2 chain of size $N = 2L$ with PBC defined as

$$|\Lambda\rangle = \frac{1}{\sqrt{\chi}} \sum_{f \in \mathcal{F}_L^{(p)}} (-1)^{|f|} |f\rangle_{1,\dots,L} \otimes |f\rangle_{L+1,\dots,2L}, \quad (1)$$

where $\mathcal{F}_L^{(p)}$ is the set of bitstrings defining the nearest neighbor Rydberg blockaded subspace for chains of L spins with PBC, $|f|$ denotes the parity of the bitstring f , and, in terms of the Fibonacci numbers F_n , $\chi = |\mathcal{F}_L^{(p)}| = F_{L-1} + F_{L+1}$ (see Fig. 1 illustrating $|\Lambda\rangle$).

By inspection, each $|f\rangle \otimes |f\rangle$ in Eq. (1) satisfies the Rydberg blockade on the full PBC chain; $|\Lambda\rangle$ is invariant under the global “particle-hole” symmetry operator $C_{\text{ph}} = \prod_{i=1}^N Z_i$ (where $Z_i \equiv |0\rangle\langle 0|_i - |1\rangle\langle 1|_i$), arbitrary

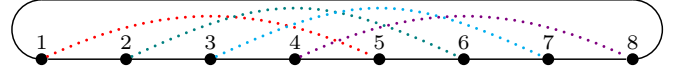


FIG. 1. State $|\Lambda\rangle$ on an $N = 2L = 8$ PBC chain. Dotted lines indicate the pairing pattern of perfectly correlated spins.

bond or site inversions, and translation by one site. It is also invariant under the pseudo-local SWAP $_{i,i+L}$ and $Z_i Z_{i+L}$ unitaries. We claim that $|\Lambda\rangle$ is an exact zero energy eigenstate of the Hamiltonian

$$H_{\text{PXP}}(N) = \sum_{i=1}^N P_{i-1} X_i P_{i+1}, \quad (i + N \equiv i), \quad (2)$$

where $P_i \equiv |0\rangle\langle 0|_i$ and $X_i \equiv |1\rangle\langle 0|_i + |0\rangle\langle 1|_i$.

For any $f \in \mathcal{F}_L^{(p)}$, the neighborhoods of spins 1 and L ($L+1$ and $2L$) are identical in $|f\rangle_{1,\dots,L}$ ($|f\rangle_{L+1,\dots,2L}$) and $|f\rangle_{1,\dots,L} \otimes |f\rangle_{L+1,\dots,2L}$ if PBC are assumed in the half-system $[1, \dots, L]$ ($[L+1, \dots, 2L]$) and the actual system $[1, \dots, 2L]$. This means that the action of $H_{\text{PXP}}(N)$ on $|\Lambda\rangle$ is equivalent to the action of the “disconnected-halves” (DH) Hamiltonian written as a sum of two decoupled PXP Hamiltonians with half-system PBC:

$$H_{\text{DH}}(L) = H_{\text{PXP}}^{\text{left}}(L)_{1,\dots,L} + H_{\text{PXP}}^{\text{right}}(L)_{L+1,\dots,2L}, \quad (3)$$

$$H_{\text{PXP}}(N) |\Lambda\rangle = H_{\text{DH}}(L) |\Lambda\rangle. \quad (4)$$

It is then easy to show that $H_{\text{PXP}}^{\text{left}}(L) |\Lambda\rangle = -H_{\text{PXP}}^{\text{right}}(L) |\Lambda\rangle$, and thus $H_{\text{PXP}}(N) |\Lambda\rangle = 0$ (see Sec. I of [25]).

The same argument holds for Hamiltonians with terms of the form $A_{[i-m,\dots,i-1]} X_i B_{[i+1,\dots,i+n]}$, where A and B are arbitrary diagonal in the computational basis operators with supports as indicated, in particular for all deformations of the PXP Hamiltonian in Refs. [8, 10, 26, 27]. Also, terms at different locations can come with different couplings as long as they are identical for sites i and $i+L$. For instance, if L is even, Hamiltonians

H_o and H_e defined by restricting the sum in Eq. (2) to, respectively, odd and even sites both annihilate $|\Lambda\rangle$, which means this state is invariant under Floquet unitaries $U_\tau^{o/e} = e^{-iH_{o/e}\tau}$ used to define the Floquet PXP model in Refs. [17, 28, 29]. In the case of extended Rydberg blockades, $\mathcal{F}_L^{(p)}$ in Eq. (1) should be substituted for bitstrings corresponding to an appropriate constrained Hilbert space. Generalizations discussed here also apply to states introduced in later sections.

Tracing over half of the chain in Eq. (1) yields the maximally mixed Gibbs ensemble of a Rydberg-blockaded PBC chain of size L (thus the von Neumann entanglement entropy $\mathcal{S}_{1/2} = \log \chi \propto L$); any observable supported on a half-system is distributed as if it is sampled from such an infinite-temperature ensemble. In contrast, non-local observables supported on $(i, i+L)$ are highly non-thermal due to perfect correlation between the spins. For a detailed discussion of the entanglement structure of $|\Lambda\rangle$ see Sec. II of [25].

Relation to other volume-entangled states.— The thermofield-double state (TFD) [30, 31], the many-body EPR state [31], and the rainbow scars [32] are also constructed on a doubled Hilbert space. In particular, $|\Lambda\rangle$ and the EPR state on the same Hilbert space differ only by parity-dependent phases. To see the connection with the rainbow scars, consider a Hamiltonian H with two decoupled real-valued in the computational basis terms acting identically on identical systems \mathcal{A} and $\bar{\mathcal{A}}$ [cf. Eq. (3)]:

$$H = H_{\mathcal{A}} + H_{\bar{\mathcal{A}}}. \quad (5)$$

As in [32], we stipulate that \mathcal{C}_{ph} is a spectral reflection symmetry [33] operator of $H_{\mathcal{A}}$ and $H_{\bar{\mathcal{A}}}$, i.e.,

$$\{H_{\mathcal{A}}, (\mathcal{C}_{\text{ph}})_{\mathcal{A}}\} = \{H_{\bar{\mathcal{A}}}, (\mathcal{C}_{\text{ph}})_{\bar{\mathcal{A}}}\} = 0. \quad (6)$$

Then, a state defined as

$$|\tilde{\Lambda}\rangle = \frac{1}{\sqrt{\dim \mathcal{K}}} \sum_{n=1}^{\dim \mathcal{K}} |\psi_n\rangle \otimes \mathcal{C}_{\text{ph}} |\psi_n\rangle, \quad (7)$$

where $|\psi_n\rangle$ are real-valued eigenstates of $H_{\mathcal{A}}$ spanning a Krylov subspace \mathcal{K} , is a zero energy eigenstate of H since $H(|\psi_n\rangle \otimes \mathcal{C}_{\text{ph}} |\psi_n\rangle) = 0$ for $\forall n$. Even though the eigenstates $|\psi_n\rangle$ are not known, we can write $|\tilde{\Lambda}\rangle$ in terms of the computational basis states spanning \mathcal{K} . Multiplying Eq. (7) by $\mathbf{1} = \sum_{f,g} |f\rangle\langle f| \otimes |g\rangle\langle g|$, where f, g are bitstrings defining the said computational basis, we obtain [using $\mathcal{C}_{\text{ph}} |g\rangle = (-1)^{|g|} |g\rangle$ and $\langle g|\psi_n\rangle \in \mathbb{R}$]

$$|\tilde{\Lambda}\rangle = \frac{1}{\sqrt{\dim \mathcal{K}}} \sum_{f:|f\rangle \in \mathcal{K}} (-1)^{|f|} |f\rangle \otimes |f\rangle, \quad (8)$$

which reproduces Eq. (1) given $\mathcal{K} = \text{span}\{|f\rangle : f \in \mathcal{F}_L^{(p)}\}$ and $H_{\mathcal{A}} = H_{\text{PXP}}(L)$. Note that $|\tilde{\Lambda}\rangle$ is a purification of the maximally mixed ensemble on \mathcal{K} .

If we interpret the decoupled Hamiltonian in Eq. (5) as H_{DH} equivalent to some “genuine” coupled (not necessarily unique) Hamiltonian with respect to its action on eigenstate $|\tilde{\Lambda}\rangle$, then finding such a genuine Hamiltonian would amount to running the argument like that leading to Eq. (3) backwards. We discuss this reverse process next.

Geometric generalization.— For concreteness, but without loss of generality, consider $|\tilde{\Lambda}\rangle = |\Lambda\rangle$, the state hosted by the PBC chain. Let us determine what PXP-type Hamiltonians of the form

$$\tilde{H}_{\text{PXP}}(G) = \sum_{i \in V} X_i \prod_{j \in V: (i,j) \in E} P_j \quad (9)$$

host it as a zero energy eigenstate. Here, $G = (V, E)$ is an undirected graph with vertices V representing spins, and edges E representing interactions — Rydberg blockades — between pairs of spins.

Per argument of the previous section, $|\tilde{\Lambda}\rangle$ is a zero-energy eigenstate of the Hamiltonian $\tilde{H}_{\text{PXP}}(G_{\mathcal{A}} \cup G_{\bar{\mathcal{A}}})$, where $G_{\mathcal{A}} \cong G_{\bar{\mathcal{A}}}$ are isomorphic graphs (ring graphs for the PBC chain) and \cup denotes a union of all vertices and edges. Let the graph isomorphism be established by the correspondence between vertices with labels i and \bar{i} , and let $|f\rangle \otimes |f\rangle$ terms in Eq. (8) be of the form $|s_1 s_2 \dots s_L\rangle_{1,2,\dots,L} \otimes |s_1 s_2 \dots s_L\rangle_{\bar{1},\bar{2},\dots,\bar{L}}$.

Due to the perfect correlation of spins i and \bar{i} , the action of $\tilde{H}_{\text{PXP}}(G_{\mathcal{A}} \cup G_{\bar{\mathcal{A}}})$ on $|\tilde{\Lambda}\rangle$ is equivalent to that of $\tilde{H}_{\text{PXP}}(G_{\mathcal{C}})$ for

$$G_{\mathcal{C}} = \left(\dots \circ \mathcal{W}_{\nu_2}^{(a_2, b_2)} \circ \mathcal{W}_{\nu_1}^{(a_1, b_1)} \right) (G_{\mathcal{A}} \cup G_{\bar{\mathcal{A}}}), \quad (10)$$

where $\mathcal{W}_{\nu}^{(a,b)}$ is the “graph modifying” operator whose non-trivial cases are

$$\begin{aligned} \mathcal{W}_+^{(a,b)}(G) &= (V, E \cup (a, \bar{b})), & \text{if } (a, b) \in E, \\ \mathcal{W}_-^{(a,b)}(G) &= (V, E \setminus (a, b)), & \text{if } (a, \bar{b}), (\bar{a}, b) \in E, \end{aligned} \quad (11)$$

with V and E being the sets of vertices and edges of G . To ensure symmetry referencing vertices of $G_{\mathcal{A}}$ and $G_{\bar{\mathcal{A}}}$, we set $\bar{\bar{i}} \equiv i$. The $\nu = “+”$ branch of $\mathcal{W}_{\nu}^{(a,b)}$ adds an intersystem interaction duplicating an already existing intrasystem interaction from the perspective of $|\tilde{\Lambda}\rangle$ [i.e., decorates the X_a operator in Eq. (9) with a superfluous for $|\tilde{\Lambda}\rangle$ projector $P_{\bar{b}} \simeq P_b$], whereas the $\nu = “-”$ branch removes an existing intrasystem interaction given a pair of equivalent for $|\tilde{\Lambda}\rangle$ intersystem interactions has been added. Thus, with respect to $|\tilde{\Lambda}\rangle$ and $\tilde{H}_{\text{PXP}}(G_{\mathcal{C}})$, $\tilde{H}_{\text{PXP}}(G_{\mathcal{A}} \cup G_{\bar{\mathcal{A}}})$ is the DH Hamiltonian.

In Fig. 2(a), we demonstrate how Eq. (10) leads from $G_{\mathcal{A}} \cup G_{\bar{\mathcal{A}}}$ to $G_{\mathcal{C}}$ corresponding to the originally considered PBC chain Hamiltonian in Eq. (2). Clearly, this construction applies generally. Given any graph $G_{\mathcal{A}}$ and a product state basis $\{|f\rangle\}$ spanning a Krylov subspace \mathcal{K}

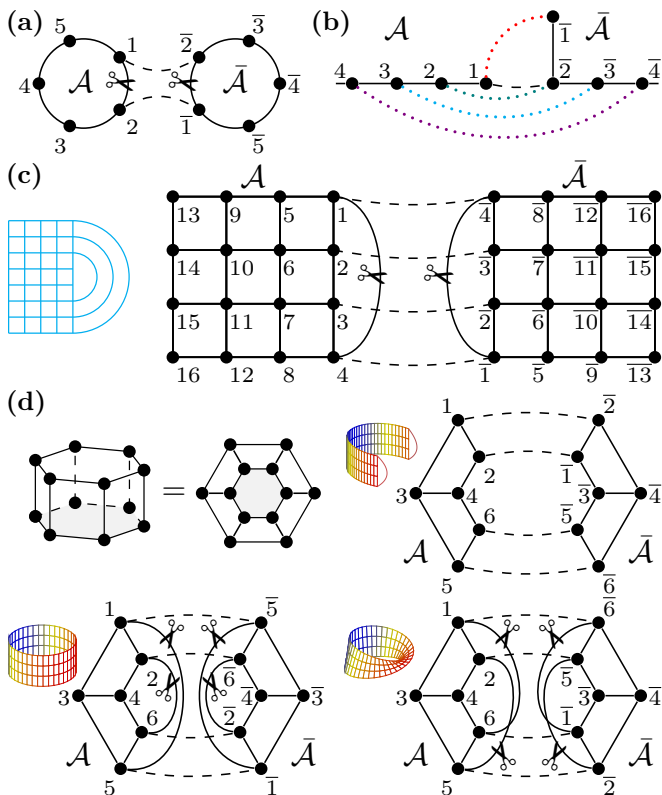


FIG. 2. Constructions of $|\tilde{\Lambda}\rangle$ -type eigenstates. The edges of graphs $G_{\mathcal{A}}$ and $G_{\bar{\mathcal{A}}}$ are solid lines; edges added via $\mathcal{W}_+^{(a,b)}$ are dashed lines; edges removed via $\mathcal{W}_-^{(a,b)}$ are indicated by the “scissors” symbol. (a) PBC chain is produced by acting on $G_{\mathcal{A}} \cup G_{\bar{\mathcal{A}}}$ with $\mathcal{W} = \mathcal{W}_-^{(\bar{1},2)} \circ \mathcal{W}_-^{(1,2)} \circ \mathcal{W}_+^{(\bar{1},2)} \circ \mathcal{W}_+^{(1,2)}$. Here $\mathcal{W}_+^{(1,2)}$ and $\mathcal{W}_+^{(\bar{1},2)}$, respectively, add edges $(1, \bar{2})$ and $(\bar{1}, 2)$ indicated with dashed lines, whereas $\mathcal{W}_-^{(1,2)}$ and $\mathcal{W}_-^{(\bar{1},2)}$ remove the edges specified in the superscripts. Clearly, $H_{\text{PXP}}(\mathcal{W}(G_{\mathcal{A}} \cup G_{\bar{\mathcal{A}}}))$ is identical to $H_{\text{PXP}}(N = 10)$ given in Eq. (2) up to the labels. (b) The dangler is generated from an OBC chain (shown as system \mathcal{A}). The dotted lines indicate the pattern of perfectly correlated spins. (c) $2L \times M$ square lattice. Although system \mathcal{A} (whose geometry for a larger system is sketched on the left) is not itself a regular square lattice, its “irregular” interactions enable the construction. When the height $M > 4$, such interactions are between sites $(1, M), (2, M - 1), \dots, (M/2 - 1, M/2 + 2)$ on top of an otherwise regular square lattice. (d) Distinct eigenstates of the PXP model on a $2L \times M$ cylinder, see text for details.

of $\tilde{H}_{\text{PXP}}(G_{\mathcal{A}})$, there exists an eigenstate of the form given in Eq. (8) hosted by $\tilde{H}_{\text{PXP}}(G_{\mathcal{A}} \cup G_{\bar{\mathcal{A}}})$ (where $G_{\bar{\mathcal{A}}} \cong G_{\mathcal{A}}$) and all (exponentially many) Hamiltonians that can be generated via Eq. (10).

A question of practical relevance is what physically reasonable systems besides the ring can host eigenstates like $|\tilde{\Lambda}\rangle$. Evidently, given any graph $G_{\mathcal{C}}$, if there exists graph $G_{\mathcal{A}}$ which generates $G_{\mathcal{C}}$ via the process prescribed by Eq. (10), then $\tilde{H}_{\text{PXP}}(G_{\mathcal{C}})$ must host an eigenstate $|\tilde{\Lambda}\rangle$ given in Eq. (8) for an appropriate Krylov subspace \mathcal{K}

of $H_{\text{PXP}}(G_{\mathcal{A}})$ (e.g., \mathcal{R} , which from now on will denote the generalized Rydberg blocked subspace of a system implied by the context).

Although no $G_{\mathcal{A}}$ generates an OBC chain (see Sec. III of [25]), an irregular OBC chain, the “dangler” shown in Fig. 2(b), can be constructed from $G_{\mathcal{A}}$ that is itself an OBC chain. The corresponding eigenstate $|\tilde{\Lambda}\rangle$ on \mathcal{R} saturates the maximal bipartite entanglement entropy attainable for the two halves. Later, using this system as an example, we will discuss experimentally and theoretically interesting dynamical properties of Hamiltonians with $|\tilde{\Lambda}\rangle$ -type eigenstates in their spectra.

Several less trivial constructions demonstrating the presence of $|\tilde{\Lambda}\rangle$ -type eigenstates in the spectra of Hamiltonians corresponding to the square lattice with OBC and cylinder (exemplified for simplicity of presentation by a PBC 2-leg ladder) are given in Figs. 2(c) and 2(d). Generically, the choice of $G_{\mathcal{A}}$ that can generate a given $G_{\mathcal{C}}$ is not unique. For instance, in Fig. 2(c) the cut could be horizontal instead of vertical, in which case $G_{\mathcal{A}}$ would be an 8×2 lattice with 3 “irregular” interactions. However, up to arbitrary labels, such construction would yield an identical geometric pairing pattern of perfectly correlated spins i and \bar{i} to the one demonstrated, and one can prove generally that the pairing pattern uniquely determines $|\tilde{\Lambda}\rangle$ on \mathcal{R} for any graph $G_{\mathcal{C}}$ (see Sec. IV of [25]).

In contrast, the PBC 2-leg ladder (with an even number of sites along the PBC dimension) allows for multiple linearly independent $|\tilde{\Lambda}\rangle$ -type eigenstates since the three choices of $G_{\mathcal{A}}$ (namely, OBC, PBC, and Möbius strip ladders) lead to distinct pairing patterns in the composite system. Note that the construction with $G_{\mathcal{A}}$ being an OBC ladder is close to that in Fig. 2(c) with the difference being that in the former case the “stitching” of the subsystems \mathcal{A} and $\bar{\mathcal{A}}$ is performed across two boundaries; the construction with a PBC ladder is similar to that in Fig. 2(a), whereas the construction with a Möbius strip is unique to this system. The PBC ladder and Möbius strip constructions yield distinct translationally invariant along the PBC direction eigenstates. The OBC ladder construction results in L linearly independent translation-symmetry-broken L -periodic eigenstates. Thus, we get the total of $L + 2$ linearly independent eigenstates residing in \mathcal{R} . The PBC and Möbius strip ladder constructions extend to the cylinder without any restriction on the height M , whereas the OBC ladder construction works only when M is even. In the latter case, $G_{\mathcal{A}}$ becomes an OBC lattice with “irregular” interactions like those in Fig. 2(c) at each boundary — also shown in the corresponding three-dimensional drawing in Fig. 2(d).

Although the three constructions in Fig. 2(d) yield globally distinct pairing patterns, some of the correlated spin pairs are shared by multiple linearly independent eigenstates, e.g., the pairs $(3, \bar{3})$ and $(4, \bar{4})$ in the OBC

ladder and Möbius strip constructions. This means that the simultaneous eigenspace of the PXP, $Z_3Z_{\bar{3}}$, and $Z_4Z_{\bar{4}}$ Hamiltonians is at least 2-dimensional. In fact, in all numerically accessible systems we probed, the dimension of the simultaneous eigenspace of $\tilde{H}_{\text{PXP}}(G_C)$ and some fixed $Z_iZ_{\bar{i}}$ on \mathcal{R} was exactly equal to the number of distinct $|\tilde{\Lambda}\rangle$ -type eigenstates with correlated spins i and \bar{i} that can be constructed on G_C . While we cannot prove that this is always true, the following theorem (proven in Sec. V of [25]) addresses one special case.

Theorem 1. *The simultaneous eigenspace of $\tilde{H}_{\text{PXP}}(G_C)$ and $Z_1Z_{\bar{1}}$ on \mathcal{R} , where G_C is the dangler graph shown in Fig. 2(b), is one-dimensional.*

We emphasize that Theorem 1 is a narrow special case of what appears to be a frequent pattern; e.g., we find numerically that the same holds for the PBC chain. The theorem is provided to demonstrate that such proofs can, in principle, be constructed, and to motivate the following discussion.

Experimental relevance.— Let G_C be the dangler geometry [Fig. 2(b)] and consider normalized eigenstates of the Hamiltonian $H_d = \tilde{H}_{\text{PXP}}(G_C)$ on \mathcal{R} written as $|\psi_n\rangle = \alpha_n |\psi_n^+\rangle + \beta_n |\psi_n^-\rangle$, where $|\psi_n^\pm\rangle$ are normalized projections onto the ± 1 eigenspaces of $Z_1Z_{\bar{1}}$; the +1 projector is $\mathcal{P}_{1\bar{1}}^+ = |00\rangle\langle 00|_{1\bar{1}} + |11\rangle\langle 11|_{1\bar{1}}$. An immediate consequence of Theorem 1 is that $\alpha_n = 1$ iff $|\psi_n\rangle = |\tilde{\Lambda}\rangle \equiv |\Lambda_d\rangle$; otherwise, $|\alpha_n| < 1$ [Fig. 3(a)]. Consider non-Hermitian operator $M_\tau = \mathcal{P}_{1\bar{1}}^+ e^{-iH_d\tau}$ that applies the projective measurement $\mathcal{P}_{1\bar{1}}^+$ after some time evolution under H_d . In Sec. VII of [25] we argue that for generic $\tau > 0$

$$\lim_{k \rightarrow \infty} M_\tau^k = |\Lambda_d\rangle\langle \Lambda_d|, \quad (12)$$

which means that postselection on the +1 outcomes of a sequence of $Z_1Z_{\bar{1}}$ measurements in the dangler system evolving under H_d converges to the projector onto the $|\Lambda_d\rangle$ eigenstate. In Fig. 3(b), we show examples of how the weight of the component of the wavefunction orthogonal to $|\Lambda_d\rangle$ becomes exponentially small in the number of successful (all resulting in the +1 outcomes) $Z_1Z_{\bar{1}}$ measurements.

The postselection probability p_k (i.e., the probability of obtaining k consecutive successful measurements) is

$$p_k = \langle \psi_{k-1} | M_\tau^\dagger M_\tau | \psi_{k-1} \rangle p_{k-1}, \quad (13)$$

where $|\psi_k\rangle = M_\tau^k |\psi_0\rangle / \|M_\tau^k |\psi_0\rangle\|$ is the normalized wavefunction after k successful measurements when one starts from the initial state $|\psi_0\rangle$. The first factor in Eq. (13) is the conditional probability of a successful k^{th} measurement given that the previous $k-1$ measurements have been successful; note that per Eq. (12) this quantity approaches 1, which means that after a long enough series of successful measurements the infidelity of the state with respect to $|\Lambda_d\rangle$ becomes expo-

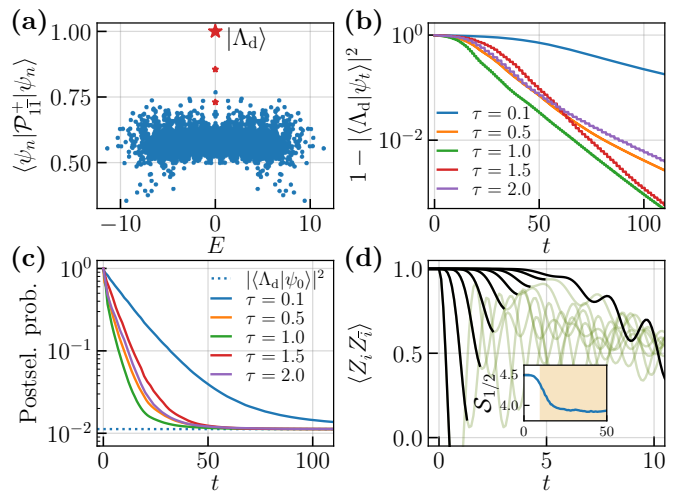


FIG. 3. Numerical study of an $N = 18$ dangler system. (a) Squared projections of eigenstates onto the +1 eigenspace of $Z_1Z_{\bar{1}}$. The smaller star markers indicate the other eigenstates in the three-fold degenerate nullspace ordered by the magnitude of the $|\psi_n^+\rangle$ component. (b),(c) State preparation via stroboscopic $Z_1Z_{\bar{1}}$ measurements separated by intervals τ (i.e., $k = \lfloor t/\tau \rfloor$ steps). Here, $|\psi_0\rangle = |00\dots 0\rangle$. The rate of exponential decrease of preparation infidelity (b) and the corresponding rate of convergence of postselection probability toward $|\langle \Lambda_d | \psi_0 \rangle|^2$ (c) depend on τ : too frequent measurements impede information scrambling in the system due to quantum Zeno effect and result in slower convergence toward $|\Lambda_d\rangle$, whereas infrequent measurements are inefficient due to allowing the system to remain in an “idle” state in which the measurement-induced information has spread away from sites 1 and $\bar{1}$. (d) Quench from the initial state $|\Lambda_d\rangle$ (here $L = 9$). The curves show successive decay of spin-spin correlations starting from $\langle Z_L Z_{\bar{L}} \rangle$ and up to $\langle Z_1 Z_{\bar{1}} \rangle$ as the “butterfly” cone spreads through the system. The inset shows the drop in the von Neumann entanglement entropy $S_{1/2}$ which results from information scrambling.

entially small in k [Fig. 3(b)] and unsuccessful measurements become extremely unlikely. As expected for repeated measurements, the recurrence in Eq. (13) gives $p_k = \langle \psi_0 | [M_\tau^\dagger]^k M_\tau^k | \psi_0 \rangle$; clearly $\lim_{k \rightarrow \infty} p_k = |\langle \Lambda_d | \psi_0 \rangle|^2$ [Fig. 3(c)].

Thus, the maximally entangled state $|\Lambda_d\rangle$ on the dangler system can be prepared via strictly local measurements of only two spins with fidelity limited only by the imperfections of the near-term Rydberg quantum devices [34–43]. In the idealized situation discussed here, benchmarking preparation fidelity of $|\Lambda_d\rangle$ can be done deterministically and without either exact or approximate classical simulations required for state-of-the-art benchmarking approaches depending on cross-entropy-based fidelity estimation [40–42, 44]. A similar protocol for preparing a rainbow eigenstate of the unconstrained 2D XY Hamiltonian was also proposed in [45].

After preparing the system in the eigenstate $|\Lambda_d\rangle$, one can study quench dynamics in the volume-entangled

regime opposite to the typical case that starts from a simple product state. For example, suppose initial state $|\Lambda_d\rangle$ is suddenly changed into another maximally entangled state $Z_L|\Lambda_d\rangle$ that is no longer an eigenstate of H_d . With L being the leftmost point of the dangler system in our labelling of sites [see Fig. 2(b)], the effect of the perturbing operator Z_L first spreads through the left half of the system, $[L, \dots, 1]$ successively destroying perfect correlations between spin pairs (i, \bar{i}) [Fig. 3(d)]. In Sec. VIII of [25] we argue that over some initial time interval the cross-subsystem correlation functions $\langle Z_i Z_{\bar{i}} \rangle$ plotted in Fig. 3(d) are directly related to the OTOC [46] $\langle [Z_i(t), Z_L(0)]^2 \rangle$, $i \in [1, \dots, L]$, for the infinite-temperature Gibbs ensemble of an OBC chain of size L (such as the subsystem \mathcal{A}); we also discuss how the OTOCs can be measured exactly using the corresponding H_{DH} . Note that our OTOC measurement protocol does not require backward time evolution (cf. Refs. [47, 48]; see [49–53] for other OTOC-related topics). In Secs. IX and X of [25] we demonstrate the stability of the state preparation and quench protocols to small perturbations, and discuss several possible practical enhancements.

Probes of quantum dynamics similar to the example discussed here do not require experimental capability beyond what is needed for preparing the system in the state $|\Lambda_d\rangle$ — in fact, state preparation appears to be the harder task among the two. Therefore, the easily verifiable ability to prepare the system in the eigenstate $|\Lambda_d\rangle$ could bolster proposals of quantum advantage on the basis of experimental probes of quantum dynamics that would be impractical to perform by means of classical computation. We conclude by noting that while we focused on the state preparation and subsequent dynamics experiments in the specific dangler geometry, we expect similar physics to hold under appropriate conditions in various other systems realizing many-body EPR states discussed in this paper.

We thank Sanjay Moudgalya, Cheng-Ju Lin, Manuel Endres, Daniel Mark, Federica Surace, Pablo Sala, Sara Vanovac, and Leo Zhou for useful discussions and previous collaborations on related topics. This work was supported by the National Science Foundation through grant DMR-2001186.

-
- [1] H. Bernien, S. Schwartz, A. Keesling, H. Levine, A. Omran, H. Pichler, S. Choi, A. S. Zibrov, M. Endres, M. Greiner, V. Vuletić, and M. D. Lukin, Probing many-body dynamics on a 51-atom quantum simulator, *Nature* **551**, 579–584 (2017).
- [2] I. Lesanovsky and H. Katsura, Interacting Fibonacci anyons in a Rydberg gas, *Phys. Rev. A* **86**, 041601 (2012).
- [3] C. J. Turner, A. A. Michailidis, D. A. Abanin, M. Serbyn, Papić, and Z. , Weak ergodicity breaking from quantum

- many-body scars, *Nature Physics* **14**, 745 (2018).
- [4] C. J. Turner, A. A. Michailidis, D. A. Abanin, M. Serbyn, and Z. Papić, Quantum scarred eigenstates in a Rydberg atom chain: Entanglement, breakdown of thermalization, and stability to perturbations, *Phys. Rev. B* **98**, 155134 (2018).
- [5] N. Shiraishi and T. Mori, Systematic construction of counterexamples to the Eigenstate Thermalization Hypothesis, *Phys. Rev. Lett.* **119**, 030601 (2017).
- [6] S. Moudgalya, S. Rachel, B. A. Bernevig, and N. Regnault, Exact excited states of nonintegrable models, *Phys. Rev. B* **98**, 235155 (2018).
- [7] S. Moudgalya, N. Regnault, and B. A. Bernevig, Entanglement of exact excited states of Affleck-Kennedy-Lieb-Tasaki models: Exact results, many-body scars, and violation of the strong eigenstate thermalization hypothesis, *Phys. Rev. B* **98**, 235156 (2018).
- [8] V. Khemani, C. R. Laumann, and A. Chandran, Signatures of integrability in the dynamics of Rydberg-blockaded chains, *Phys. Rev. B* **99**, 161101 (2019).
- [9] C.-J. Lin and O. I. Motrunich, Exact quantum many-body scar states in the Rydberg-blockaded atom chain, *Phys. Rev. Lett.* **122**, 173401 (2019).
- [10] S. Choi, C. J. Turner, H. Pichler, W. W. Ho, A. A. Michailidis, Z. Papić, M. Serbyn, M. D. Lukin, and D. A. Abanin, Emergent SU(2) dynamics and perfect quantum many-body scars, *Phys. Rev. Lett.* **122**, 220603 (2019).
- [11] F. M. Surace, P. P. Mazza, G. Giudici, A. Lerose, A. Gambassi, and M. Dalmonte, Lattice gauge theories and string dynamics in Rydberg atom quantum simulators, *Phys. Rev. X* **10**, 021041 (2020).
- [12] T. Iadecola, M. Schecter, and S. Xu, Quantum many-body scars from magnon condensation, *Phys. Rev. B* **100**, 184312 (2019).
- [13] N. Shiraishi, Connection between quantum-many-body scars and the Affleck–Kennedy–Lieb–Tasaki model from the viewpoint of embedded Hamiltonians, *Journal of Statistical Mechanics: Theory and Experiment* **2019**, 083103 (2019).
- [14] K. Omiya and M. Müller, Quantum many-body scars in bipartite Rydberg arrays originating from hidden projector embedding, *Phys. Rev. A* **107**, 023318 (2023).
- [15] K. Omiya and M. Müller, Fractionalization paves the way to local projector embeddings of quantum many-body scars, *Phys. Rev. B* **108**, 054412 (2023).
- [16] M. Ljubotina, J.-Y. Desaulles, M. Serbyn, and Z. Papić, Superdiffusive energy transport in kinetically constrained models, *Phys. Rev. X* **13**, 011033 (2023).
- [17] G. Giudici, F. M. Surace, and H. Pichler, Unraveling PXP many-body scars through Floquet dynamics (2023), [arXiv:2312.16288](https://arxiv.org/abs/2312.16288).
- [18] M. Serbyn, D. A. Abanin, and Z. Papić, Quantum many-body scars and weak breaking of ergodicity, *Nature Physics* **17**, 675–685 (2021).
- [19] Z. Papić, Weak ergodicity breaking through the lens of quantum entanglement, in *Entanglement in Spin Chains: From Theory to Quantum Technology Applications*, edited by A. Bayat, S. Bose, and H. Johanneson (Springer International Publishing, Cham, 2022) pp. 341–395.
- [20] S. Moudgalya, B. A. Bernevig, and N. Regnault, Quantum many-body scars and Hilbert space fragmentation: a review of exact results, *Reports on Progress in Physics* **85**, 086501 (2022).

- [21] A. Chandran, T. Iadecola, V. Khemani, and R. Moessner, Quantum many-body scars: A quasiparticle perspective, *Annual Review of Condensed Matter Physics* **14**, 443 (2023).
- [22] S. Moudgalya and O. I. Motrunich, Exhaustive characterization of quantum many-body scars using commutator algebras (2023), [arXiv:2209.03377 \[cond-mat.str-el\]](https://arxiv.org/abs/2209.03377).
- [23] C.-J. Lin, V. Calvera, and T. H. Hsieh, Quantum many-body scar states in two-dimensional Rydberg atom arrays, *Phys. Rev. B* **101**, 220304 (2020).
- [24] A. A. Michailidis, C. J. Turner, Z. Papić, D. A. Abanin, and M. Serbyn, Stabilizing two-dimensional quantum scars by deformation and synchronization, *Phys. Rev. Res.* **2**, 022065 (2020).
- [25] Supplemental material (2024).
- [26] V. Karle, M. Serbyn, and A. A. Michailidis, Area-law entangled eigenstates from nullspaces of local Hamiltonians, *Phys. Rev. Lett.* **127**, 060602 (2021).
- [27] F. M. Surace, M. Votto, E. G. Lazo, A. Silva, M. Dalmonte, and G. Giudici, Exact many-body scars and their stability in constrained quantum chains, *Phys. Rev. B* **103**, 104302 (2021).
- [28] T. Iadecola and S. Vijay, Nonergodic quantum dynamics from deformations of classical cellular automata, *Phys. Rev. B* **102**, 180302 (2020).
- [29] P.-G. Rozon, M. J. Gullans, and K. Agarwal, Constructing quantum many-body scar Hamiltonians from Floquet automata, *Phys. Rev. B* **106**, 184304 (2022).
- [30] W. Cottrell, B. Freivogel, D. M. Hofman, and S. F. Lokhande, How to build the thermofield double state, *Journal of High Energy Physics* **2019**, 58 (2019).
- [31] J. Wildeboer, C. M. Langlett, Z.-C. Yang, A. V. Gorshkov, T. Iadecola, and S. Xu, Quantum many-body scars from Einstein-Podolsky-Rosen states in bilayer systems, *Phys. Rev. B* **106**, 205142 (2022).
- [32] C. M. Langlett, Z.-C. Yang, J. Wildeboer, A. V. Gorshkov, T. Iadecola, and S. Xu, Rainbow scars: From area to volume law, *Phys. Rev. B* **105**, L060301 (2022).
- [33] M. Schechter and T. Iadecola, Many-body spectral reflection symmetry and protected infinite-temperature degeneracy, *Phys. Rev. B* **98**, 035139 (2018).
- [34] H. Labuhn, D. Barredo, S. Ravets, S. de Léséleuc, T. Macrì, T. Lahaye, and A. Browaeys, Tunable two-dimensional arrays of single Rydberg atoms for realizing quantum ising models, *Nature* **534**, 667–670 (2016).
- [35] A. Browaeys and T. Lahaye, Many-body physics with individually controlled Rydberg atoms, *Nature Physics* **16**, 132–142 (2020).
- [36] E. Altman, K. R. Brown, G. Carleo, L. D. Carr, E. Demler, C. Chin, B. DeMarco, S. E. Economou, M. A. Eriksson, K.-M. C. Fu, M. Greiner, K. R. Hazzard, R. G. Hulet, A. J. Kollár, B. L. Lev, M. D. Lukin, *et al.*, Quantum simulators: Architectures and opportunities, *PRX Quantum* **2**, 017003 (2021).
- [37] S. Ebadi, A. Keesling, M. Cain, T. T. Wang, H. Levine, D. Bluvstein, G. Semeghini, A. Omran, J.-G. Liu, R. Samajdar, X.-Z. Luo, B. Nash, X. Gao, B. Barak, E. Farhi, S. Sachdev, *et al.*, Quantum optimization of maximum independent set using Rydberg atom arrays, *Science* **376**, 1209 (2022).
- [38] D. Bluvstein, S. J. Evered, A. A. Geim, S. H. Li, H. Zhou, T. Manovitz, S. Ebadi, M. Cain, M. Kalinowski, D. Hangleiter, J. P. Bonilla Ataides, N. Maskara, I. Cong, X. Gao, P. Sales Rodriguez, *et al.*, Logical quantum processor based on reconfigurable atom arrays, *Nature* **626**, 58–65 (2023).
- [39] I. S. Madjarov, J. P. Covey, A. L. Shaw, J. Choi, A. Kale, A. Cooper, H. Pichler, V. Schkolnik, J. R. Williams, and M. Endres, High-fidelity entanglement and detection of alkaline-earth Rydberg atoms, *Nature Physics* **16**, 857–861 (2020).
- [40] J. Choi, A. L. Shaw, I. S. Madjarov, X. Xie, R. Finkelstein, J. P. Covey, J. S. Cotler, D. K. Mark, H.-Y. Huang, A. Kale, H. Pichler, F. G. S. L. Brandão, S. Choi, and M. Endres, Preparing random states and benchmarking with many-body quantum chaos, *Nature* **613**, 468–473 (2023).
- [41] D. K. Mark, J. Choi, A. L. Shaw, M. Endres, and S. Choi, Benchmarking quantum simulators using ergodic quantum dynamics, *Phys. Rev. Lett.* **131**, 110601 (2023).
- [42] A. L. Shaw, Z. Chen, J. Choi, D. K. Mark, P. Scholl, R. Finkelstein, A. Elben, S. Choi, and M. Endres, Benchmarking highly entangled states on a 60-atom analog quantum simulator (2023), [arXiv:2308.07914](https://arxiv.org/abs/2308.07914).
- [43] S. Anand, C. E. Bradley, R. White, V. Ramesh, K. Singh, and H. Bernien, A dual-species Rydberg array (2024), [arXiv:2401.10325](https://arxiv.org/abs/2401.10325).
- [44] F. Arute, K. Arya, R. Babbush, D. Bacon, J. Bardin, R.arends, R. Biswas, S. Boixo, F. Brandao, D. Buell, B. Burkett, Y. Chen, J. Chen, B. Chiaro, R. Collins, *et al.*, Quantum supremacy using a programmable superconducting processor, *Nature* **574**, 505–510 (2019).
- [45] L. Agarwal, C. M. Langlett, and S. Xu, Long-range Bell states from local measurements and many-body teleportation without time reversal, *Phys. Rev. Lett.* **130**, 020801 (2023).
- [46] S. Xu and B. Swingle, Scrambling dynamics and out-of-time-ordered correlators in quantum many-body systems, *PRX Quantum* **5**, 010201 (2024).
- [47] B. Sundar, A. Elben, L. K. Joshi, and T. V. Zache, Proposal for measuring out-of-time-ordered correlators at finite temperature with coupled spin chains, *New Journal of Physics* **24**, 023037 (2022).
- [48] A. M. Green, A. Elben, C. H. Alderete, L. K. Joshi, N. H. Nguyen, T. V. Zache, Y. Zhu, B. Sundar, and N. M. Linke, Experimental measurement of out-of-time-ordered correlators at finite temperature, *Phys. Rev. Lett.* **128**, 140601 (2022).
- [49] B. Swingle, G. Bentsen, M. Schleier-Smith, and P. Hayden, Measuring the scrambling of quantum information, *Phys. Rev. A* **94**, 040302 (2016).
- [50] N. Y. Yao, F. Grusdt, B. Swingle, M. D. Lukin, D. M. Stamper-Kurn, J. E. Moore, and E. A. Demler, Interferometric approach to probing fast scrambling (2016), [arXiv:1607.01801 \[quant-ph\]](https://arxiv.org/abs/1607.01801).
- [51] C. B. Dağ and L.-M. Duan, Detection of out-of-time-order correlators and information scrambling in cold atoms: Ladder-XX model, *Phys. Rev. A* **99**, 052322 (2019).
- [52] B. Yoshida and N. Y. Yao, Disentangling scrambling and decoherence via quantum teleportation, *Phys. Rev. X* **9**, 011006 (2019).
- [53] D. Yuan, S.-Y. Zhang, Y. Wang, L.-M. Duan, and D.-L. Deng, Quantum information scrambling in quantum many-body scarred systems, *Phys. Rev. Res.* **4**, 023095 (2022).

Supplemental Material: Volume-entangled exact eigenstates in the PXP and related models in any dimension

Andrew N. Ivanov and Olexei I. Motrunich
*Department of Physics and Institute for Quantum Information and Matter,
 California Institute of Technology, Pasadena, California 91125, USA*
 (Dated: April 15, 2024)

I. PROOF $|\Lambda\rangle$ IS AN EIGENSTATE OF $H_{\text{PXP}}(N)$

In this section we show that $|\Lambda\rangle$ in Eq. (1) is an eigenstate of the Hamiltonian $H_{\text{DH}}(L)$ in Eq. (3) and, therefore, a zero energy eigenstate of $H_{\text{PXP}}(N)$ in Eq. (2). Up to normalization,

$$H_{\text{PXP}}^{\text{left}}(L) |\Lambda\rangle = \sum_{f \in \mathcal{F}_L^{(p)}} (-1)^{|f|} [H_{\text{PXP}}(L) |f\rangle] \otimes |f\rangle, \quad (\text{S1a})$$

$$H_{\text{PXP}}^{\text{right}}(L) |\Lambda\rangle = \sum_{f \in \mathcal{F}_L^{(p)}} (-1)^{|f|} |f\rangle \otimes [H_{\text{PXP}}(L) |f\rangle]. \quad (\text{S1b})$$

Eqs. (S1a) and (S1b) multiplied by resolutions of identity $\left(\sum_{g \in \mathcal{F}_L^{(p)}} |g\rangle\langle g|\right)_{1, \dots, L}$ and $\left(\sum_{g \in \mathcal{F}_L^{(p)}} |g\rangle\langle g|\right)_{L+1, \dots, 2L}$, respectively, give

$$H_{\text{PXP}}^{\text{left}}(L) |\Lambda\rangle = \sum_{f, g \in \mathcal{F}_L^{(p)}} \gamma(f, g) |g\rangle \otimes |f\rangle, \quad (\text{S2a})$$

$$H_{\text{PXP}}^{\text{right}}(L) |\Lambda\rangle = \sum_{f, g \in \mathcal{F}_L^{(p)}} \gamma(f, g) |f\rangle \otimes |g\rangle, \quad (\text{S2b})$$

where $\gamma(f, g) = (-1)^{|f|} \langle g | H_{\text{PXP}}(L) | f \rangle$. Note that it is acceptable for the terms in the resolutions of identity above to satisfy the half-system Rydberg blockade for PBC and not OBC because, by construction, $H_{\text{DH}}(L)$ acting on $|\Lambda\rangle$ does not produce any components that violate the PBC Rydberg blockade for any half of the system.

Since $\langle g | H_{\text{PXP}}(L) | f \rangle \neq 0$ iff $|f| \neq |g| \pmod 2$, it follows, per real-valuedness of $H_{\text{PXP}}(L)$ in this basis, that $\gamma(f, g) = -\gamma(g, f)$ and therefore $H_{\text{PXP}}^{\text{left}}(L) |\Lambda\rangle = -H_{\text{PXP}}^{\text{right}}(L) |\Lambda\rangle$. Thus $H_{\text{PXP}}(N) |\Lambda\rangle = H_{\text{DH}}(L) |\Lambda\rangle = 0$.

II. ENTANGLEMENT STRUCTURE OF $|\Lambda\rangle$

In this section we summarize various results characterizing entanglement in the state $|\Lambda\rangle$ on the PBC chain. From the form of Eq. (1) we immediately see that the cut across two opposite bonds that produces two identical subsystems of size L has Schmidt index χ with all the Schmidt values equal to $\chi^{-1/2}$. Therefore, the entanglement entropy between such half-systems is $\mathcal{S}_{1/2} = \log \chi$, which is linear in the system size for large N . Moreover, for any bipartition of an arbitrary system subject to Rydberg blockade into two separately connected subsystems of equal size (i.e., the subsystems that remain connected even if all intersystem bonds are removed), $\mathcal{S}_{1/2} \leq \log |\mathcal{F}_L^{(o)}|$, where $|\mathcal{F}_L^{(o)}| = F_{L+2}$ is the cardinality of the set $\mathcal{F}_L^{(o)}$ containing all bitstrings defining the Rydberg-blockaded subspace \mathcal{R} for systems of L spins with open boundary conditions (OBC). It is easy to show that $\log |\mathcal{F}_L^{(o)}| - \log \chi \rightarrow -\log(\varphi^{-3} + \varphi^{-1}) \approx 0.16$ for large N , where $\varphi = (1 + \sqrt{5})/2$ is the golden ratio. Thus $|\Lambda\rangle$ has the highest rate of half-system entanglement entropy growth with N attainable on \mathcal{R} whenever a system is partitioned into two individually connected subsystems.

Clearly, taking a partial trace over one half of the system results in a diagonal reduced density matrix (RDM) proportional to the identity. In fact, any partial trace of the form $\rho_m = \text{Tr}_B |\Lambda\rangle\langle\Lambda|$, where subsystem B is a geometrically connected subset of $N - m \geq N/2$ sites is diagonal; by definition

$$\rho_m = \sum_{\substack{f \in \mathcal{F}_L^{(p)}, \\ g = f_{[m+1 \dots L]}}} (\mathbf{1}_m \otimes \langle gf |) |\Lambda\rangle\langle\Lambda| (\mathbf{1}_m \otimes |gf\rangle) = \frac{1}{\chi} \sum_{\substack{f \in \mathcal{F}_L^{(p)}, \\ h = f_{[1 \dots m]}}} |h\rangle\langle h| = \frac{1}{\chi} \sum_{h \in \mathcal{F}_m^{(o)}} \alpha_m(h) |h\rangle\langle h|, \quad (\text{S3})$$

where

$$\alpha_m(h) = F_{L-m+2-(h_1+h_m)}. \quad (\text{S4})$$

In particular,

$$\rho_1 = \frac{1}{\chi} (F_{L+1} |0\rangle\langle 0| + F_{L-1} |1\rangle\langle 1|), \quad (\text{S5})$$

which in the thermodynamic limit yields the following RDM corresponding to an infinite-temperature Gibbs ensemble:

$$\rho_1^\infty = \frac{1}{\sqrt{5}} (\varphi |0\rangle\langle 0| + \varphi^{-1} |1\rangle\langle 1|). \quad (\text{S6})$$

From Eqs. (S3) and (S4) we see that ρ_m will have F_{m+2} diagonal entries (corresponding to the cardinality of $\mathcal{F}_m^{(o)}$), of which F_m entries with $h_1 + h_m = 0$ will have $\alpha_m(h) = F_{L-m+2}$; $2F_{m-1}$ entries with $h_1 + h_m = 1$ will have $\alpha_m(h) = F_{L-m+1}$; and F_{m-2} entries with $h_1 + h_m = 2$ will have $\alpha_m(h) = F_{L-m}$. Thus the Von Neumann entanglement entropy with respect to a bipartition into contiguous subsystems of sizes $m \in [1 \dots L]$ and $N - m$ is

$$\begin{aligned} \mathcal{S}(\rho_m) &= -\text{Tr}[\rho_m \log \rho_m] \\ &= -\frac{1}{\chi} \left(F_m F_{L-m+2} \log \frac{F_{L-m+2}}{\chi} + 2F_{m-1} F_{L-m+1} \log \frac{F_{L-m+1}}{\chi} + F_{m-2} F_{L-m} \log \frac{F_{L-m}}{\chi} \right). \end{aligned} \quad (\text{S7})$$

For the last equation to be valid for $m = 1$ and $m = L$, we need to assume that $F_{-1} = 1$ (true for the extension of the Fibonacci numbers to negative integers given by $F_{-n} = (-1)^{n+1} F_n$), and that $0 \cdot \log 0 = 0$. It follows from the discussion above that $F_m F_{L-m+2} + 2F_{m-1} F_{L-m+1} + F_{m-2} F_{L-m} = \chi \cdot \text{Tr} \rho_m = \chi$ and, therefore, Eq. (S7) can also be written in a form that is more suitable for the case when m is close to L as follows:

$$\mathcal{S}(\rho_m) = \log \chi - \frac{1}{\chi} (F_m F_{L-m+2} \log F_{L-m+2} + 2F_{m-1} F_{L-m+1} \log F_{L-m+1} + F_{m-2} F_{L-m} \log F_{L-m}). \quad (\text{S8})$$

In the thermodynamic limit, for any finite m , it is possible to show using exact expressions for F_m, F_{m-1}, F_{m-2} and asymptotic expressions for $F_{L-m+2}, F_{L-m+1}, F_{L-m}$ that are exponentially accurate in L that Eq. (S7) reduces to

$$\mathcal{S}(\rho_m) = \left(m - \frac{2\varphi}{\sqrt{5}} \right) \log \varphi + \frac{1}{2} \log 5, \quad (\text{S9})$$

indicating that entanglement entropy of $|\Lambda\rangle$ grows according to the volume law.

Next, let us consider non-local bipartitions. Of particular interest are those where one of the subsystems consists of two spins separated by some distance ℓ , which we can take to be spins 1 and $1 + \ell$ w.l.o.g. and write the corresponding RDM as $\rho[1; 1 + \ell]$. Note that $|\Lambda\rangle$ is an eigenstate of the two-qubit SWAP gate acting on any two spins separated by distance L , which means that $\rho[1; 1 + \ell] = \rho[1; 1 + \ell \pm L]$. Therefore, for any $\ell \neq L$ we can consider the two spins to be from the same contiguous half-system, and it follows from Eq. (S3) that

$$\rho[1; 1 + \ell] = \rho[1; 1 + (\ell \bmod L)] = \sum_{s, s' \in \{0,1\}} \beta_\ell(s, s') |ss'\rangle\langle ss'|, \quad \ell \neq L, \quad (\text{S10})$$

where coefficients $\beta_\ell(s, s')$ result from taking a partial trace over a subsystem of size $L - 2$, which excludes the specific spins at positions 1 and $1 + \ell$, of an infinite-temperature Gibbs ensemble of size L . Thus for all pairs of spins in $|\Lambda\rangle$, except those separated by distance $l = L$, RDMs are diagonal mixtures of product states.

For spins separated by distance $l = L$ the situation is very different. To simplify the analysis, let us reorder the spins in $|\Lambda\rangle$ as follows: $|s_1 s_2 \dots s_L\rangle^{\otimes 2} \rightarrow |s_1 s_1\rangle \otimes |s_2 \dots s_L\rangle^{\otimes 2}$. Then in this reordered basis $|\Lambda\rangle$ can be written as

$$|\Lambda\rangle = \sum_{g \in \mathcal{F}_{L-1}^{(o)}} (-1)^{|g|} (|00\rangle - \delta_{g_1,0} \delta_{g_{L-1},0} |11\rangle) \otimes |g\rangle^{\otimes 2}. \quad (\text{S11})$$

Taking a partial trace over the last $N - 2$ spins, one gets two-site density matrix for sites 1 and L

$$\rho[1; 1 + L] = \frac{1}{\chi} [F_{L-1} (|00\rangle - |11\rangle) (\langle 00| - \langle 11|) + F_L |00\rangle\langle 00|], \quad (\text{S12})$$

which for sufficiently large L is very close to

$$\lim_{L \rightarrow \infty} \rho[1; 1+L] = \frac{1}{\sqrt{5}\varphi} (\varphi^2 |00\rangle\langle 00| + |11\rangle\langle 11| - |00\rangle\langle 11| - |11\rangle\langle 00|). \quad (\text{S13})$$

Note that reduction from Eq. (S13) to single-spin RDM is in agreement with Eq. (S6).

In contrast with the rainbow scars constructed in [32], the entanglement ‘‘bonds’’ cut by any contiguous bipartition of $|\Lambda\rangle$ are not perfect Bell pairs. The corresponding RDM in the large size limit, $\lim_{L \rightarrow \infty} \rho[1; L+1]$, is a mixed state composed of two less-than-maximally entangled states, which up to normalization can be written as

$$\begin{aligned} |\xi_1\rangle &= 2|00\rangle - \eta|11\rangle, \\ |\xi_2\rangle &= \eta|00\rangle + 2|11\rangle, \end{aligned} \quad (\text{S14})$$

where $\eta = \sqrt{\varphi^4 - 2\varphi^2 + 5} - \varphi \approx 0.9545$; the eigenvalue associated with $|\xi_1\rangle$ in $\lim_{L \rightarrow \infty} \rho[1; L+1]$ is $p_1 = (2\varphi^2 + \eta)/(2\sqrt{5}\varphi) \approx 0.856$. The discrepancy between the entanglement structure of $|\Lambda\rangle$ and that of the rainbow state is entirely due to the fact that we restricted the former to \mathcal{R} , where the dynamical constraint makes each individual spin (and, by extension, any subsystem) of PXP model’s eigenstates entangled with the rest of the system — e.g., as shown by Eq. (S6). Such a restriction, obviously inessential to the general construction, was chosen due to its relevance for experiments with Rydberg atom arrays. By substituting $\mathcal{F}_L^{(p)}$ with $\{0, 1\}^L$ in Eq. (1) we get a zero energy eigenstate of $H_{\text{PXP}}(N)$ in the space free from any dynamical constraint. This eigenstate would be more rainbow-like; in particular, repeating the above analysis, one can easily show that $\rho_{1,L}$ will change from the mixed state given in Eqs. (S12)–(S14) to a pure Bell state proportional to $|00\rangle - |11\rangle$.

III. NO $|\tilde{\Lambda}\rangle$ -TYPE STATES ON OBC CHAINS

Suppose G_C is a chain of length $2L$ with open boundary conditions (OBC). Note that any sequence of operators in Eq. (11) cannot decrease the initial degree of a vertex in $G_{\mathcal{A}} \cup G_{\bar{\mathcal{A}}}$. Hence one vertex in $G_{\mathcal{A}}$ must have a degree of 1, whereas all other vertices must have a degree of at most 2. Since obtaining the connected G_C is impossible unless $G_{\mathcal{A}}$ is connected, $G_{\mathcal{A}}$ must be an OBC chain consisting of L sites; let these sites have labels $1, 2, \dots, L$. The only way to produce G_C , then, is to combine $G_{\mathcal{A}}$ and $G_{\bar{\mathcal{A}}}$ with a single edge $(a, \bar{b}) \in \{(1, \bar{1}), (1, \bar{L}), (L, \bar{1}), (L, \bar{L})\}$; i.e., by acting with $\mathcal{W}_+^{(a,b)}$. However, such $\mathcal{W}_+^{(a,b)}$ could act only if edge $(a, b) \in \{(1, 1), (1, L), (L, 1), (L, L)\}$ is in $G_{\mathcal{A}}$, which (unless $L = 2$) is not possible.

IV. UNIQUENESS OF $|\tilde{\Lambda}\rangle$ ON \mathcal{R} FROM GLOBAL PAIRING PATTERN

In this section we show that no two eigenstates on the Rydberg blockade subspace \mathcal{R} of $\tilde{H}_{\text{PXP}}(G_C)$ (with G_C being an arbitrary graph with $N = 2L$ vertices) can share the same global pairing pattern of perfectly correlated spins. Given any fixed pairing of sites into L distinct pairs (i, \bar{i}) , there can exist at most one eigenstate of $\tilde{H}(G_C)$ characterized by it.

Lemma 2. *If $|\psi\rangle \in \mathcal{R}$ is a simultaneous eigenstate of $\tilde{H}_{\text{PXP}}(G_C)$ and $Z_i Z_{\bar{i}}$ for a given i , then $|\psi\rangle$ must be annihilated by $\mathcal{P}_{\mathcal{R}}(X_i + X_{\bar{i}})$, where $\mathcal{P}_{\mathcal{R}}$ is a projector onto \mathcal{R} , or, equivalently, $|\psi\rangle$ must be annihilated by the the sum of two terms of $\tilde{H}_{\text{PXP}}(G_C)$ that have an X operator acting on spins at sites i or \bar{i} .*

Proof. If $|\psi\rangle$ is a simultaneous eigenstate of $\tilde{H}_{\text{PXP}}(G_C)$ and $Z_i Z_{\bar{i}}$, it must be annihilated by

$$[\tilde{H}_{\text{PXP}}(G_C), Z_i Z_{\bar{i}}] = \mathcal{P}_{\mathcal{R}}([X_i, Z_i] Z_{\bar{i}} + Z_i [X_{\bar{i}}, Z_{\bar{i}}]) \propto \mathcal{P}_{\mathcal{R}}(Y_i Z_{\bar{i}} + Z_i Y_{\bar{i}}), \quad (\text{S15})$$

and hence by

$$Z_i Z_{\bar{i}} [\tilde{H}_{\text{PXP}}(G_C), Z_i Z_{\bar{i}}] \propto \mathcal{P}_{\mathcal{R}}(X_i + X_{\bar{i}}). \quad (\text{S16})$$

In the above manipulations we used the fact that $[\mathcal{P}_{\mathcal{R}}, Z_i Z_{\bar{i}}] = 0$. \square

Theorem 3. *If $|\psi\rangle \in \mathcal{R}$ is an eigenstate of $\tilde{H}_{\text{PXP}}(G_C)$ and*

$$Z_i Z_{\bar{i}} |\psi\rangle = |\psi\rangle \quad \text{for } \forall i \in [1..L], \quad (\text{S17})$$

it must have zero energy and be unique.

Proof. Eq. (S17) restricts $|\psi\rangle$ to the form

$$|\psi\rangle = \sum_{|f\rangle \in \mathcal{K}} c_f |f\rangle \otimes |f\rangle, \quad (\text{S18})$$

where c_f are some coefficients and $\mathcal{K} \subset \mathbb{C}^{2^L}$ is a subspace spanned by computational basis states $|f\rangle$ such that $|f\rangle \otimes |f\rangle \in \mathcal{R}$. Thus, $\mathcal{C}_{\text{ph}}|\psi\rangle = |\psi\rangle$ — i.e., $|\psi\rangle$ has definite parity. This is only possible if $|\psi\rangle$ has zero energy.

Per Lemma 2, $|\psi\rangle$ must be annihilated by $\mathcal{P}_{\mathcal{R}}(X_i + X_{\bar{i}})$ for $\forall i \in [1..L]$, which gives

$$\mathcal{P}_{\mathcal{R}}(X_i + X_{\bar{i}}) |\psi\rangle = \mathcal{P}_{\mathcal{R}} \sum_{|f\rangle \in \mathcal{K}} c_f [(X_i |f\rangle) \otimes |f\rangle + |f\rangle \otimes (X_{\bar{i}} |f\rangle)] = 0. \quad (\text{S19})$$

Taking an inner product of both sides Eq. (S19) with an arbitrary state $\langle s| \otimes \langle t| \in \mathcal{R}^*$ we get

$$\sum_{|f\rangle \in \mathcal{K}} (c_f \langle s|X_i|f\rangle \langle t|f\rangle + c_f \langle s|f\rangle \langle t|X_{\bar{i}}|f\rangle) = 0, \quad (\text{S20})$$

where we used X_i instead of $X_{\bar{i}}$ since the labels are arbitrary in expressions involving a half-system. Equation (S20) can be written as

$$c_t \langle s|X_i|t\rangle + c_s \langle t|X_i|s\rangle = (c_s + c_t) \langle s|X_i|t\rangle = 0. \quad (\text{S21})$$

A somewhat subtle point is that in going from Eq. (S20) to Eq. (S21) we implicitly restricted $|s\rangle$ and $|t\rangle$ to subspace \mathcal{K} . This is, of course, not problematic since given the form of Eq. (S18) \mathcal{K} is exactly the subspace of interest.

Suppose $|t|$ is the Hamming weight (number of ones in bitstring t) of some $|t\rangle \in \mathcal{K}$. Consider the set $\Omega_t^- = \{|q\rangle : |q\rangle = X_i |t\rangle \text{ and } |q| = |t| - 1\}$. Clearly $\Omega_t^- = \emptyset$ iff $|t\rangle = |00\dots 0\rangle$; otherwise, Ω_t^- is a nonempty set and $\Omega_t^- \subset \mathcal{K}$. This means for $\forall |t\rangle \in \mathcal{K}$, $|t| > 0 \exists |q_1\rangle \in \Omega_t^-$, which then implies $c_{q_1} + c_t = 0$. But then if $|q_1| > 0$, $\exists |q_2\rangle \in \Omega_{q_1}^-$, implying $c_{q_2} + c_{q_1} = 0$, and so on. This recurrence terminates at $|q_{|t|-1}| = 1$ yielding $c_{q_{|t|}} + c_{q_{|t|-1}} = 0$, where $q_{|t|} = |00\dots 0\rangle$. Using these relations we obtain

$$c_t = (-1)^{|t|} \cdot c_{00\dots 0}. \quad (\text{S22})$$

Since $|t\rangle \in \mathcal{K}$ was arbitrary, we conclude that every amplitude in Eq. (S18) is related to $c_{00\dots 0}$. Thus, after plugging c_t given in Eq. (S22) into Eq. (S18) and normalizing we get a unique state formally identical to $|\tilde{\Lambda}\rangle$ given in Eq. (8) of the main text. \square

We note that the above argument for the uniqueness of the $|\tilde{\Lambda}\rangle$ -type state for a given global pairing pattern holds for any PXP-type model on any graph G_C , but it does not guarantee that the state exists as an eigenstate (hence we had to assume it does). By examining the proof we can also formulate a simple sufficient condition for the eigenstate to exist in the Rydberg-blockaded subspace \mathcal{R} of $\tilde{H}_{\text{PXP}}(G_C)$ referencing only the G_C and the global pairing $\{(i, \bar{i})\}$, which, naturally, defines two subgraphs $\tilde{G}_{\mathcal{A}}$ and $\tilde{G}_{\bar{\mathcal{A}}}$ with the same number of vertices but not necessarily the same structure. We also assume that the graph G_C does not contain edges connecting i and \bar{i} for every i (otherwise the corresponding spins would be fixed as $|00\rangle_{i\bar{i}}$ in the $|\tilde{\Lambda}\rangle$ -type state, which is not interesting). Consider sets $\Omega_i = \{j, (i, j) \in E\}$ and $\Omega_{\bar{i}} = \{j, (\bar{i}, j) \in E\}$ for $\forall i$. Given an arbitrary G_C , these sets can contain vertices belonging to both subgraphs $\tilde{G}_{\mathcal{A}}$ and $\tilde{G}_{\bar{\mathcal{A}}}$. Let us introduce function $u(v)$ that acts as identity on the vertices $\tilde{G}_{\mathcal{A}}$, but maps vertices of $\tilde{G}_{\bar{\mathcal{A}}}$ to the corresponding vertices of $\tilde{G}_{\mathcal{A}}$ (e.g., $u(\bar{1}) = 1$, but $u(1) = 1$). Now, a sufficient condition for the existence of a $|\tilde{\Lambda}\rangle$ -type state given a global pairing pattern is the following:

$$\{u(j), j \in \Omega_i\} = \{u(j), j \in \Omega_{\bar{i}}\} \equiv \tilde{\Omega}_i. \quad (\text{S23})$$

In the wavefunction amplitude language as in the above uniqueness proof, this condition implies that, for any i and any $|g\rangle_{\text{rest}}$, we have two non-trivial possibilities: either both $|00\rangle_{i\bar{i}} |g\rangle_{\text{rest}} |g\rangle_{\text{rest}}$ and $|11\rangle_{i\bar{i}} |g\rangle_{\text{rest}} |g\rangle_{\text{rest}}$ are in \mathcal{R} and hence contribute to $|\tilde{\Lambda}\rangle$ with opposite amplitudes, in which case their total contribution is annihilated by $\mathcal{P}_{\mathcal{R}}(X_i + X_{\bar{i}})$; or $|00\rangle_{i\bar{i}} |g\rangle_{\text{rest}} |g\rangle_{\text{rest}}$ is in \mathcal{R} but $|11\rangle_{i\bar{i}} |g\rangle_{\text{rest}} |g\rangle_{\text{rest}}$ is not due to blockades at i and \bar{i} provided by the rest of the spins, in which case only the former contributes to $|\tilde{\Lambda}\rangle$ and this contribution is annihilated by both $\mathcal{P}_{\mathcal{R}}X_i$ and $\mathcal{P}_{\mathcal{R}}X_{\bar{i}}$ due to the same blockades by the rest as guaranteed by the above condition. Hence $\mathcal{P}_{\mathcal{R}}(X_i + X_{\bar{i}}) |\tilde{\Lambda}\rangle = 0$.

In the graph language, the condition of Eq. (S23) effectively says that G_C can be constructed from two isomorphic graphs $G_{\mathcal{A}}$ and $G_{\bar{\mathcal{A}}}$ (sharing all the vertices, but not necessarily edges, with, respectively, $\tilde{G}_{\mathcal{A}}$ and $\tilde{G}_{\bar{\mathcal{A}}}$) via the construction of Eq. (10) in the main text. Given the condition is satisfied, we can define graph $G_{\mathcal{A}}$ explicitly as follows: $G_{\mathcal{A}} = (V_{\mathcal{A}}, \{(i, j), i \in V_{\mathcal{A}} \text{ and } j \in \tilde{\Omega}_i\})$, where $V_{\mathcal{A}}$ are the vertices of $\tilde{G}_{\mathcal{A}}$. Then the said $|\tilde{\Lambda}\rangle$ -type state will purify the maximally mixed ensemble on \mathcal{R} of $\tilde{H}_{\text{PXP}}(G_{\mathcal{A}})$ on the system with the Hamiltonian $\tilde{H}_{\text{PXP}}(G_C)$.

V. UNIQUENESS OF THE EIGENSTATE OF $Z_1 Z_{\bar{1}}$ ON \mathcal{R} ON THE ‘‘DANGLER’’ CONFIGURATION

Our goal in this section is to show that there is only one eigenstate of the PXP model on the dangler geometry that is also a +1 eigenstate of $Z_1 Z_{\bar{1}}$, namely the $|\tilde{\Lambda}\rangle$ -type state from the main text. Note that this is a much stronger statement than in the preceding section since we are requiring that only one pair of sites, 1 and $\bar{1}$, is correlated.

Suppose G_C is the ‘‘dangler’’ graph [Fig. 2(b) in the main text] with $N = 2L$ vertices, and $H_{\text{PXP}} = \tilde{H}_{\text{PXP}}(G_C)$. The proof, established mainly via the following two lemmas, will lie in showing that any +1 eigenstate of $Z_1 Z_{\bar{1}}$ must be characterized by a global pairing pattern.

Lemma 4. *If $|\psi\rangle$ is an eigenstate of H_{PXP} and $Z_1 Z_{\bar{1}} |\psi\rangle = |\psi\rangle$ then $|\psi\rangle$ must be a +1 eigenstate of $Z_2 Z_{\bar{2}}$.*

Proof. Per Lemma 2, $|\psi\rangle$ must be annihilated by

$$H_1 = P_2 X_1 P_2 + X_{\bar{1}} P_{\bar{2}}. \quad (\text{S24})$$

Note that at this point we cannot assume anything about the relationship between spins at sites 2 and $\bar{2}$.

Let us write $|\psi\rangle$ as

$$|\psi\rangle = \sum_{s_2 s_1 s_{\bar{2}} \in \mathcal{F}_3^{(o)}} |s_1 s_1\rangle_{1, \bar{1}} |s_2 s_{\bar{2}}\rangle_{2, \bar{2}} |\tilde{\phi}_{s_2 s_1 s_{\bar{2}}}\rangle_{\text{rest}}, \quad (\text{S25})$$

where $|\tilde{\phi}_{s_2 s_1 s_{\bar{2}}}\rangle_{\text{rest}}$ are unnormalized wavefunctions defined on the subsystem consisting of all spins except those with labels 1, $\bar{1}$, 2, $\bar{2}$. For conciseness, in what follows we will drop the subscripts indicating the subsystems on the kets in the above tensor product, always understanding them appearing in the same order as in the above. From

$$H_1 |\psi\rangle = |10\rangle |00\rangle |\tilde{\phi}_{000}\rangle + |01\rangle |00\rangle |\tilde{\phi}_{000}\rangle + |01\rangle |10\rangle |\tilde{\phi}_{100}\rangle + |10\rangle |00\rangle |\tilde{\phi}_{010}\rangle + |01\rangle |00\rangle |\tilde{\phi}_{010}\rangle = 0, \quad (\text{S26})$$

we deduce that

$$|\tilde{\phi}_{000}\rangle = -|\tilde{\phi}_{010}\rangle, \quad (\text{S27a})$$

$$|\tilde{\phi}_{100}\rangle = 0. \quad (\text{S27b})$$

While Eq. (S27a) gives us little useful information at this point, Eq. (S27b) says that components with spins 2 and $\bar{2}$ in states, respectively, $|1\rangle$ and $|0\rangle$ are forbidden. Thus the only term in Eq. (S25) that is not a +1 eigenstate of $Z_2 Z_{\bar{2}}$ is the one with $s_2 s_1 s_{\bar{2}} = 001$. To prove the Lemma we need to show that it must vanish as well.

Let us write $|\psi\rangle$ explicitly utilizing everything we have learned about its form so far:

$$|\psi\rangle = |00\rangle \left(|00\rangle |\tilde{\phi}_{000}\rangle + |01\rangle |\tilde{\phi}_{001}\rangle + |11\rangle |\tilde{\phi}_{101}\rangle \right) - |11\rangle |00\rangle |\tilde{\phi}_{000}\rangle, \quad (\text{S28})$$

where we used the result of Eq. (S27a) to write the last term. Consider the individual unnormalized terms in Eq. (S28):

$$|\tilde{\psi}_{00}\rangle = |00\rangle \left(|00\rangle |\tilde{\phi}_{000}\rangle + |01\rangle |\tilde{\phi}_{001}\rangle + |11\rangle |\tilde{\phi}_{101}\rangle \right), \quad (\text{S29a})$$

$$|\tilde{\psi}_{11}\rangle = |11\rangle |00\rangle |\tilde{\phi}_{000}\rangle. \quad (\text{S29b})$$

Thus,

$$|\psi\rangle = |\tilde{\psi}_{00}\rangle - |\tilde{\psi}_{11}\rangle. \quad (\text{S30})$$

Now, $|\psi\rangle$ must be an eigenstate of the Hamiltonian

$$H' = H_{\text{PXP}} - H_1 \quad (\text{S31})$$

with the same eigenvalue λ as that in $H_{\text{PXP}} |\psi\rangle = \lambda |\psi\rangle$. Since H' doesn't modify spins 1 and $\bar{1}$, and therefore doesn't mix $|\tilde{\psi}_{00}\rangle$ and $|\tilde{\psi}_{11}\rangle$, we conclude that

$$H' |\tilde{\psi}_{00}\rangle = \lambda |\tilde{\psi}_{00}\rangle, \quad (\text{S32a})$$

$$H' |\tilde{\psi}_{11}\rangle = \lambda |\tilde{\psi}_{11}\rangle. \quad (\text{S32b})$$

Let us rewrite Eq. (S32b) explicitly as follows:

$$H' |\tilde{\psi}_{11}\rangle = |11\rangle \left[(H' - H_2) |00\rangle |\tilde{\phi}_{000}\rangle \right] = \lambda |11\rangle |00\rangle |\tilde{\phi}_{000}\rangle, \quad (\text{S33})$$

where H_2 denotes terms of H' with X operators acting on sites 2 and $\bar{2}$; i.e.,

$$H_2 = P_3 X_2 P_1 + P_1 P_{\bar{1}} X_2 P_3. \quad (\text{S34})$$

From Eq. (S33) — which is correct because $H_2 |\tilde{\psi}_{11}\rangle = 0$ and $H' - H_2$ has no support on sites 1 and $\bar{1}$ — we deduce that

$$(H' - H_2) |00\rangle_{2,\bar{2}} |\tilde{\phi}_{000}\rangle = \lambda |00\rangle_{2,\bar{2}} |\tilde{\phi}_{000}\rangle. \quad (\text{S35})$$

Note that the wavefunction in Eq. (S35) is defined on the subsystem that excludes sites 1 and $\bar{1}$.

Let us now write the action of H' on $|\tilde{\psi}_{00}\rangle$ in a rather strange fashion for reasons to become apparent shortly:

$$H' |\tilde{\psi}_{00}\rangle = H_2 |00\rangle |00\rangle |\tilde{\phi}_{000}\rangle \quad (\text{S36})$$

$$+ |00\rangle \left[(H' - H_2) |00\rangle |\tilde{\phi}_{000}\rangle \right] \quad (\text{S37})$$

$$+ H_2 |00\rangle |01\rangle |\tilde{\phi}_{001}\rangle \quad (\text{S38})$$

$$+ |00\rangle \left[(H' - H_2) |01\rangle |\tilde{\phi}_{001}\rangle \right] \quad (\text{S39})$$

$$+ H' |00\rangle |11\rangle |\tilde{\phi}_{101}\rangle. \quad (\text{S40})$$

Acting with projector $\mathcal{P}_{0000} = |0000\rangle\langle 0000|_{1\bar{1}2\bar{2}}$ on both sides of Eq. (S32a), we get

$$\mathcal{P}_{0000} H' |\tilde{\psi}_{00}\rangle = \lambda |00\rangle |00\rangle |\tilde{\phi}_{000}\rangle. \quad (\text{S41})$$

Now, given the form of Eq. (S36), it is clear that \mathcal{P}_{0000} will annihilate all terms except those in lines labeled as Eqs. (S37) and (S38). Thus

$$\mathcal{P}_{0000} H' |\tilde{\psi}_{00}\rangle = |00\rangle \left[(H' - H_2) |00\rangle |\tilde{\phi}_{000}\rangle \right] + |00\rangle |00\rangle |\tilde{\phi}_{001}\rangle. \quad (\text{S42})$$

where in the last line we used $P_3 |\tilde{\phi}_{001}\rangle = |\tilde{\phi}_{001}\rangle$ by Rydberg blockade on $\bar{3}$ from excited state at $\bar{1}$. Combining Eqs. (S35), (S41), and (S42), we obtain

$$\lambda |00\rangle |00\rangle |\tilde{\phi}_{000}\rangle + |00\rangle |00\rangle |\tilde{\phi}_{001}\rangle = \lambda |00\rangle |00\rangle |\tilde{\phi}_{000}\rangle \implies |\tilde{\phi}_{001}\rangle = 0. \quad (\text{S43})$$

In the above analysis we silently assumed that $L > 2$. In the special case when $L = 2$, $H' - H_2 = 0$, $|\tilde{\phi}_{s_2 s_1 s_2}\rangle_{\text{rest}}$ are just numbers, and one arrives at exactly the same conclusion following similar steps. \square

Lemma 5. *If $|\psi\rangle$ is an eigenstate of H_{PXP} and $Z_i Z_{\bar{i}} |\psi\rangle = |\psi\rangle$ for $\forall i \in [1, \dots, m]$, where $2 \leq m < L$, then $|\psi\rangle$ must also be a +1 eigenstate of $Z_{m+1} Z_{m+1}$.*

Proof. First, consider the case of $m = 2$. We want to show that $|\psi\rangle$ must be an eigenstate of $Z_3 Z_{\bar{3}}$ ($L \geq 3$). Per Lemma 2, $|\psi\rangle$ must be annihilated by the following operators:

$$H_1 = P_2 X_1 P_2 + X_{\bar{1}} P_2 \simeq P_2 X_1 + X_{\bar{1}} P_2, \quad (\text{S44a})$$

$$H_2 = P_3 X_2 P_1 + P_1 P_{\bar{1}} X_2 P_3 \simeq P_3 X_2 P_1 + P_{\bar{1}} X_2 P_3, \quad (\text{S44b})$$

where in the expressions to the right of \simeq , we removed redundant projectors as far as acting on $|\psi\rangle$ is concerned.

Let us express $|\psi\rangle$ as

$$|\psi\rangle = \sum_{s_1 s_2 \in \mathcal{F}_2^{(o)}} |s_1 s_1\rangle_{1,\bar{1}} |s_2 s_2\rangle_{2,\bar{2}} |\tilde{\phi}_{s_1 s_2}\rangle, \quad (\text{S45})$$

where $|\tilde{\phi}_{s_1 s_2}\rangle$ are unnormalized wavefunctions defined on the subsystem consisting of all spins except those with labels 1, $\bar{1}$, 2, $\bar{2}$. Note that of the three terms in Eq. (S45) the one with $s_1 s_2 = 01$ is already a +1 eigenstate of $Z_3 Z_{\bar{3}}$; i.e.,

$$Z_3 Z_{\bar{3}} |\tilde{\phi}_{01}\rangle = |\tilde{\phi}_{01}\rangle \quad (\text{S46})$$

because spins 3 and $\bar{3}$ are forced to be in the state $|0\rangle$ by the adjacent spins 2 and $\bar{2}$ in the state $|1\rangle$.

With spins in the same order as in Eq. (S45), the action of H_2 on $|\psi\rangle$ can be written as

$$H_2 |\psi\rangle = |00\rangle \left[|01\rangle \left(|\tilde{\phi}_{01}\rangle + P_3 |\tilde{\phi}_{00}\rangle \right) + |10\rangle \left(|\tilde{\phi}_{01}\rangle + P_3 |\tilde{\phi}_{00}\rangle \right) \right], \quad (\text{S47})$$

where we have used $P_3 |\tilde{\phi}_{01}\rangle = P_{\bar{3}} |\tilde{\phi}_{01}\rangle = |\tilde{\phi}_{01}\rangle$. For H_2 to annihilate $|\psi\rangle$ the following two conditions must be satisfied:

$$P_3^0 |\tilde{\phi}_{00}\rangle = -|\tilde{\phi}_{01}\rangle, \quad (\text{S48a})$$

$$P_{\bar{3}}^0 |\tilde{\phi}_{00}\rangle = -|\tilde{\phi}_{01}\rangle. \quad (\text{S48b})$$

Clearly, using $P_j = (1 - Z_j)/2$, this is only possible if $|\tilde{\phi}_{00}\rangle$ does not have any components where spins 3 and $\bar{3}$ are in different states. Thus we conclude that

$$Z_3 Z_{\bar{3}} |\tilde{\phi}_{00}\rangle = |\tilde{\phi}_{00}\rangle. \quad (\text{S49})$$

Finally, acting with H_1 on $|\psi\rangle$ we get

$$H_1 |\psi\rangle = (|10\rangle |00\rangle + |01\rangle |00\rangle) (|\tilde{\phi}_{00}\rangle + |\tilde{\phi}_{10}\rangle), \quad (\text{S50})$$

which gives $|\tilde{\phi}_{10}\rangle = -|\tilde{\phi}_{00}\rangle$ and, therefore,

$$Z_3 Z_{\bar{3}} |\tilde{\phi}_{10}\rangle = |\tilde{\phi}_{10}\rangle. \quad (\text{S51})$$

Combining Eqs. (S45), (S46), (S49), and (S51) we conclude that

$$Z_3 Z_{\bar{3}} |\psi\rangle = |\psi\rangle. \quad (\text{S52})$$

Suppose the conditions of the Lemma are satisfied up to some $m > 2$. Then $|\psi\rangle$ must be annihilated by operators H_1, H_2, \dots, H_m , analogous to the ones given in Eqs. (S44a) and (S44b). We can express $|\psi\rangle$ as

$$|\psi\rangle = \sum_{s_1, s_2, \dots, s_m \in \mathcal{F}_m^{(\sigma)}} |s_1 \dots s_{m-2}\rangle_{1, \dots, m-2} |s_1 \dots s_{m-2}\rangle_{\bar{1}, \dots, m-2} |s_{m-1} s_m\rangle_{m-1, m-1} |s_m s_m\rangle_{m, \bar{m}} |\tilde{\phi}_{s_{m-1} s_m}^{s_1 \dots s_{m-2}}\rangle, \quad (\text{S53})$$

where $|\tilde{\phi}_{s_{m-1} s_m}^{s_1 \dots s_{m-2}}\rangle$ are unnormalized wavefunctions defined on the subsystem consisting of all spins except those with labels $1, \bar{1}, 2, \bar{2}, \dots, m, \bar{m}$. Now, via arguments identical to the ones we used in the $m = 2$ case applied to individual wavefunction parts with any fixed $s_1 s_2 \dots s_{m-2}$ one can show that

$$Z_{m+1} Z_{m+1} |\tilde{\phi}_{s_{m-1} s_m}^{s_1 \dots s_{m-2}}\rangle = |\tilde{\phi}_{s_{m-1} s_m}^{s_1 \dots s_{m-2}}\rangle. \quad (\text{S54})$$

Specifically, if $s_{m-2} = 0$, the argument is entirely identical with H_m replacing H_2 and H_{m-1} replacing H_1 ; whereas if $s_{m-2} = 1$, then $s_{m-1} s_m$ can only take values 00 and 01, which means Eq. (S54) follows from only requiring that H_m annihilate $|\psi\rangle$. \square

We are now ready to prove the main result:

Theorem 6. *The simultaneous eigenspace of $\tilde{H}_{PXP}(G_C)$ and $Z_1 Z_{\bar{1}}$ on \mathcal{R} is one-dimensional.*

Proof. Per Lemma 4, any state $|\psi\rangle$ in the simultaneous eigenspace of $\tilde{H}_{PXP}(G_C)$ and $Z_1 Z_{\bar{1}}$ must be an eigenstate of $Z_2 Z_{\bar{2}}$. Then, by induction on the result of Lemma 5, $|\psi\rangle$ must also be an eigenstate of $Z_i Z_{\bar{i}}$ for any $i \in [1, \dots, L]$. Hence by Theorem 3, $|\psi\rangle$ must have zero energy and be unique. Since a state $|\Lambda_d\rangle$ satisfying the conditions of the Theorem has been constructed explicitly in the main text, the unique $|\psi\rangle$ discussed herein exists. \square

VI. UNIQUENESS OF THE EIGENSTATE OF $Z_1 Z_{\bar{1}}$ ON TWO IDENTICAL DECOUPLED OBC CHAINS

In this section we establish the same result as that obtained in the previous section for the dangler, but for a simpler system consisting of two identical decoupled OBC chains.

Suppose $G_{\mathcal{A}}$ and $G_{\bar{\mathcal{A}}}$ are isomorphic OBC chains of size L (i.e., $G_{\mathcal{A}} \cup G_{\bar{\mathcal{A}}}$ is the decoupled system that generates the dangler). Before we proceed, let us remark that Lemma 5 applies without modification to the system considered here (one simply needs to assume the simplification made in Eq. (S44a) from the start); hence, we will invoke Lemma 5 in what follows.

Theorem 7. *The simultaneous eigenspace of $\tilde{H}_{PXP}(G_{\mathcal{A}} \cup G_{\bar{\mathcal{A}}})$ and $Z_1 Z_{\bar{1}}$ on \mathcal{R} is one-dimensional.*

Proof. Per Lemma 2, $|\psi\rangle$ must be annihilated by

$$H_1 = P_2 X_1 + X_{\bar{1}} P_2. \quad (\text{S55})$$

Consider $|\psi\rangle$ expressed in the form given by Eq. (S25). From

$$H_1 |\psi\rangle = |10\rangle |00\rangle |\tilde{\phi}_{000}\rangle + |10\rangle |01\rangle |\tilde{\phi}_{001}\rangle + |01\rangle |00\rangle |\tilde{\phi}_{010}\rangle + |01\rangle |00\rangle |\tilde{\phi}_{000}\rangle + |01\rangle |10\rangle |\tilde{\phi}_{100}\rangle + |10\rangle |00\rangle |\tilde{\phi}_{010}\rangle = 0,$$

we deduce that

$$|\tilde{\phi}_{000}\rangle = -|\tilde{\phi}_{010}\rangle, \quad |\tilde{\phi}_{001}\rangle = |\tilde{\phi}_{100}\rangle = 0. \quad (\text{S56})$$

Hence $|\psi\rangle$ is a +1 eigenstate of $Z_2 Z_{\bar{2}}$, which implies, by induction on the result of Lemma 5, that $|\psi\rangle$ is characterized by a global pairing pattern such that $Z_i Z_{\bar{i}} |\psi\rangle = |\psi\rangle$ for $\forall i \in [1, \dots, L]$. The rest of the argument is entirely identical to that used in Theorem 6. \square

In particular, this result implies that the same state $|\Lambda_d\rangle$, whose preparation was described in the main text using projective $Z_1 Z_{\bar{1}}$ measurements and dynamics under the dangler PXP model, can also be prepared on decoupled OBC chains through an identical protocol (this is illustrated in Figs. S1(a) and S1(b)).

VII. COMPOSITE EVOLUTION AND PROJECTIVE MEASUREMENT OPERATOR M_τ

In this section we want to justify Eq. (12) in the main text. We assume there exists a provably unique state $|\Lambda\rangle$ that is a simultaneous eigenstate of some PXP-type Hamiltonian H and projective measurement operator $\mathcal{P}_{1\bar{1}}^+$. The discussion easily generalizes to the case of multiple states $|\Lambda_1\rangle, |\Lambda_2\rangle, \dots, |\Lambda_n\rangle$ with the same properties.

We first describe an intuitive argument.

Due to its non-Hermiticity, operator M_τ is not particularly easy to work with. We can, however, express M_τ^k as a product of k Hermitian operators and a unitary using the following structure:

$$M_\tau^k = e^{-kiH\tau} \times e^{kiH\tau} \mathcal{P}_{1\bar{1}}^+ e^{-kiH\tau} \times \dots \times e^{2iH\tau} \mathcal{P}_{1\bar{1}}^+ e^{-2iH\tau} \times e^{iH\tau} \mathcal{P}_{1\bar{1}}^+ e^{-iH\tau}. \quad (\text{S57})$$

Note that in the context of amplitude damping (of anything orthogonal to $|\Lambda\rangle$) by M_τ^k the leftmost unitary $e^{-kiH\tau}$ has no effect and thus can be ignored. We can, therefore, view M_τ^k as a product of Hermitian Heisenberg operators $\mathcal{P}_{1\bar{1}}^+(t) = e^{iHt} \mathcal{P}_{1\bar{1}}^+ e^{-iHt}$ written as

$$M_\tau^k \simeq \mathcal{P}_{1\bar{1}}^+(k\tau) \dots \mathcal{P}_{1\bar{1}}^+(2\tau) \mathcal{P}_{1\bar{1}}^+(\tau). \quad (\text{S58})$$

Clearly, $\sigma_{\mathcal{P}_{1\bar{1}}^+(t)} = \sigma_{\mathcal{P}_{1\bar{1}}^+}$, where σ_T denotes the spectrum of an operator T ; i.e., the spectra of all the operators in Eq. (S58) are identical and contain only 0's and 1's. Let V_t^λ , where $\lambda \in \{0, 1\}$, be the time-dependent eigenspace of $\mathcal{P}_{1\bar{1}}^+(t)$ corresponding to eigenvalue λ , $V_t^\lambda = e^{iHt} V_0^\lambda$; therefore, $\mathcal{P}_{1\bar{1}}^+(t)$ is a projector $\mathcal{H} \rightarrow V_t^1$, where $\mathcal{H} = V_t^0 \oplus V_t^1$ is the full Hilbert space. For any two times t_1 and t_2 , and any λ ,

$$V_{t_1}^\lambda \cap V_{t_2}^\lambda \subseteq V_{t_1}^\lambda, \quad V_{t_1}^\lambda \cap V_{t_2}^\lambda \subseteq V_{t_2}^\lambda \quad (\text{S59})$$

Given the overall chaotic nature of the PXP Hamiltonian and only a single common eigenstate with $\mathcal{P}_{1\bar{1}}^+$, it is reasonable to assume that for generic $t_1 \neq t_2$, $V_{t_1}^\lambda \cap V_{t_2}^\lambda$ will be a proper subset of both $V_{t_1}^\lambda$ and $V_{t_2}^\lambda$. In other words, subspaces $V_{t_1}^\lambda$ and $V_{t_2}^\lambda$ will not be exactly equal; and if the interval between t_1 and t_2 is sufficiently large, these subspaces can

be considered to occupy random regions of the full Hilbert space. Although each operator in Eq. (S59) has exactly $\dim V_0^1$ fixed points with eigenvalue 1, there is only one fixed point which is guaranteed to be shared among all these operators, namely $|\Lambda\rangle$. This, together with the assumption that equality is almost never obtained in Eq. (S59) for any consecutive times $t_1 = q\tau$ and $t_2 = (q+1)\tau$, we conclude that M_τ^k is a projector $\mathcal{H} \rightarrow V_\tau^1 \cap V_{2\tau}^1 \cap \dots \cap V_{k\tau}^1$, which in the limit of large k converges to $\mathcal{H} \rightarrow \text{span}\{|\Lambda\rangle\}$.

This picture provides some insights into how state preparation dynamics depends on the interval between measurements [see Figs. 3(b) and S1(a)]. The reason one cannot speed up state preparation via too frequent (small τ) measurements is that subspaces $V_{q\tau}^1$ and $V_{(q+1)\tau}^1 = e^{iH\tau}V_{q\tau}^1$ almost perfectly overlap, which does not allow for significant leakage of any amplitude out of the time-dependent $\lambda = 1$ sector; the system becomes semi-confined in its original subspace projected onto V_τ^1 in a way reminiscent of the quantum Zeno effect. On the other hand, in the case of infrequent measurements (large generic τ), $V_{q\tau}^1 \cap V_{(q+1)\tau}^1$ is, effectively, an overlap between two random subspaces in the full Hilbert space. The average rate of amplitude leakage per measurement as τ gets large is expected to saturate at some purely geometric quantity, so infrequent measurements simply result in a poor “duty cycle.”

Above, we reasoned in the operator picture without regard to states. We now present a complementary point of view thinking more in terms of states. Consider subspace orthogonal to $|\Lambda\rangle$, which we will denote W . Both P_{11}^+ and H act within W , hence the same is true for M_τ , and all the action below will be understood within W . We want to see if generically $|\mu| < 1$ for all eigenvalues μ of M_τ in W . Note that the operator M_τ is non-Hermitian, but we can still find its (in general complex) eigenvalues and bring it to the Jordan normal form using a similarity transformation. Hence, if all $|\mu| < 1$, with finite Jordan blocks (true for finite-dimensional Hilbert spaces), then large powers of this operator decay to zero, i.e., $\lim_{k \rightarrow \infty} M_\tau^k W = 0$. Note that there is no contradiction between $\|M_\tau\| = 1$ (which follows from earlier arguments) and eigenvalues of M_τ satisfying $|\mu| < 1$: $\|M_\tau\|$ is related to eigenvalues of $(M_\tau^\dagger M_\tau)^{1/2}$, which are not simply related to eigenvalues of M_τ for non-Hermitian M_τ . On the other hand, those earlier arguments do not impose conditions on $\|M_\tau^k\|$ in W , and the Jordan normal form arguments show that it will decay to zero for large k if all $|\mu| < 1$.

Suppose μ is an eigenvalue of M_τ in W and $|\Phi\rangle \in W$ is the corresponding eigenstate, $M_\tau |\Phi\rangle = \mu |\Phi\rangle$ (i.e., $|\Phi\rangle$ is a right eigenvector of M_τ). Since $\|M_\tau |\Phi\rangle\| \leq \|\Phi\|$, we must have $|\mu| \leq 1$. Suppose we have $|\mu| = 1$. Let us denote $|\Theta\rangle = e^{-iH\tau} |\Phi\rangle$. We have $\|\Theta\rangle\| = \|\Phi\rangle\|$ and $P_{11}^+ |\Theta\rangle = \mu |\Phi\rangle$, and since we have assumed $|\mu| = 1$ and P_{11}^+ is a projector, we must have $P_{11}^+ |\Theta\rangle = |\Theta\rangle$. The eigenvector condition $M_\tau |\Phi\rangle = \mu |\Phi\rangle$ then implies $|\Theta\rangle = \mu |\Phi\rangle$, i.e., $e^{-iH\tau} |\Phi\rangle = \mu |\Phi\rangle$, which in turn means that $P_{11}^+ |\Phi\rangle = |\Phi\rangle$. Thus, $|\Phi\rangle$ is a simultaneous eigenstate of P_{11}^+ (with eigenvalue +1), and of $e^{-iH\tau}$. Hence, if we can argue that P_{11}^+ and $e^{-iH\tau}$ do not have simultaneous eigenstates in W , we obtain a contradiction, implying that $|\mu|$ cannot be equal to 1 and hence must be smaller than 1.

By the assumed uniqueness of $|\Lambda\rangle$, we know that P_{11}^+ and H cannot have simultaneous eigenstates in W . This does not yet mean the same for P_{11}^+ and $e^{-iH\tau}$, since we may have a situation where an eigenstate of P_{11}^+ is, e.g., a superposition of two eigenstates of H with distinct eigenvalues ϵ and ϵ' that happen to produce $e^{-i\epsilon\tau} = e^{-i\epsilon'\tau}$, and then this superposition is also an eigenstate of $e^{-iH\tau}$. This situation clearly requires fine-tuning of τ , as well as more special properties of H like the above superposition of two eigenstates of H being an eigenstate of P_{11}^+ . Intuitively, even properties like the latter are unlikely for a generic chaotic Hamiltonian H ; however, we do not need to assume this to see that for most values of τ we will have $e^{-i\epsilon\tau} \neq e^{-i\epsilon'\tau}$ for distinct eigenvalues $\epsilon \neq \epsilon'$, and the above essentially covers any adversarial situation leading to there being simultaneous eigenstates of P_{11}^+ and $e^{-iH\tau}$ in W . A more formal argument is as follows. Suppose $\{\epsilon_n\}$ are distinct eigenvalues of H with degeneracies $\{d_n\}$ and the corresponding eigenspaces $\{W_n\}$, $W = \oplus_n W_n$. As long as we are dealing with finite sets (true for finite systems), clearly, for most choices of τ the corresponding phase values $\{e^{-i\tau\epsilon_n}\}$ will be distinct (possible τ violating this being measure zero). These are then distinct eigenvalues of $e^{-iH\tau}$, and the corresponding eigenspaces are also uniquely fixed to be $\{W_n\}$. Hence any eigenstate of $e^{-iH\tau}$ must be within one of the W_n 's and hence must also be an eigenstate of H . Hence, any common eigenstate of P_{11}^+ and $e^{-iH\tau}$ in W is also an eigenstate of H , which is not allowed.

Note that in these more formal arguments we require τ to be away from some special fine-tuned values that depend on the system size, and we also considered the limit $k \rightarrow \infty$ while keeping the dimension of the Hilbert space fixed, which however becomes exponentially large with the system size. While we cannot prove it, more suggestive earlier arguments and chaoticity of H likely make the situation better producing reasonable convergence of $M_\tau^k W$ to zero for any generic τ and that does not require k exponentially large in system size. In the end, our numerical studies of the state preparation in the main text is the strong and most practical evidence for this.

VIII. MEASUREMENT OF THE OUT-OF-TIME-ORDER CORRELATION (OTOC) FUNCTIONS USING $|\bar{\Lambda}\rangle$ -TYPE STATES

In this section we start by justifying the claim made in the main text that for short enough time $t < t_B$ (where t_B is the “butterfly” time to be defined more precisely later) the two-point correlators $\langle Z_i Z_{\bar{i}} \rangle = \langle \psi(t) | Z_i Z_{\bar{i}} | \psi(t) \rangle$ measured as a function of time t in the quench experiment with $|\psi(t=0)\rangle = Z_L |\Lambda\rangle$ in Fig. 3(d) are equivalent to the four-point out-of-time-order correlation (OTOC) function [49]

$$F(t) = \left\langle W_t^\dagger V^\dagger W_t V \right\rangle, \quad (\text{S60})$$

where $W_t = Z_L(t)$ and $V = Z_i$, and the average is taken with respect to the infinite-temperature Gibbs ensemble of an OBC chain of size L . We will then also show that the same protocol, when applied to identical decoupled OBC chains, allows measuring exact OTOCs for any time t . We will conclude the section with a short discussion on the more general applicability of our protocol to systems with different geometric configurations.

Denoting the unitary evolution by operator $U_t = e^{-iH_d t}$, the argument goes as follows:

$$\langle Z_i Z_{\bar{i}} \rangle = \text{Tr} \left(Z_i Z_{\bar{i}} U_t Z_L |\Lambda_d\rangle \langle \Lambda_d| Z_L U_t^\dagger \right) \quad (\text{S61a})$$

$$= \text{Tr} \left(Z_i Z_{\bar{i}} U_t Z_L U_t^\dagger |\Lambda_d\rangle \langle \Lambda_d| U_t Z_L U_t^\dagger \right) \quad (\text{S61b})$$

$$= \text{Tr} \left(Z_i Z_{\bar{i}} Z_L(-t) |\Lambda_d\rangle \langle \Lambda_d| Z_L(-t) \right) \quad (\text{S61c})$$

$$= \text{Tr} \left(Z_L(-t) Z_i Z_{\bar{i}} Z_L(-t) |\Lambda_d\rangle \langle \Lambda_d| \right) \quad (\text{S61d})$$

$$= \text{Tr} \left(Z_L(-t) Z_i Z_{\bar{i}} Z_L(-t) Z_i Z_{\bar{i}} |\Lambda_d\rangle \langle \Lambda_d| \right) \quad (\text{S61e})$$

$$\stackrel{t < t_B}{\simeq} \text{Tr} \left(Z_L(-t) Z_i Z_L(-t) Z_i |\Lambda_d\rangle \langle \Lambda_d| \right) \quad (\text{S61f})$$

$$= \text{Tr} \left(Z_L(-t) Z_i Z_L(-t) Z_i |\Lambda_d\rangle \langle \Lambda_d| \right) \quad (\text{S61g})$$

$$= \text{Tr}_{\mathcal{A}} \text{Tr}_{\bar{\mathcal{A}}} \left(Z_L(-t) Z_i Z_L(-t) Z_i |\Lambda_d\rangle \langle \Lambda_d| \right) \quad (\text{S61h})$$

$$= \text{Tr}_{\mathcal{A}} \sum_{f \in \mathcal{F}_L^{(o)}} \left(\mathbf{1}_{\mathcal{A}} \otimes \langle f |_{\bar{\mathcal{A}}} [Z_L(-t) Z_i Z_L(-t) Z_i |\Lambda_d\rangle \langle \Lambda_d|] \mathbf{1}_{\mathcal{A}} \otimes |f\rangle_{\bar{\mathcal{A}}} \right) \quad (\text{S61i})$$

$$\stackrel{t < t_B}{\simeq} \text{Tr}_{\mathcal{A}} \left(Z_L(-t) Z_i Z_L(-t) Z_i \sum_{f \in \mathcal{F}_L^{(o)}} \left[\mathbf{1}_{\mathcal{A}} \otimes \langle f |_{\bar{\mathcal{A}}} |\Lambda_d\rangle \langle \Lambda_d| \mathbf{1}_{\mathcal{A}} \otimes |f\rangle_{\bar{\mathcal{A}}} \right] \right) \quad (\text{S61j})$$

$$= \text{Tr}_{\mathcal{A}} \left(Z_L(-t) Z_i Z_L(-t) Z_i \frac{1}{|\mathcal{F}_L^{(o)}|} \sum_{f \in \mathcal{F}_L^{(o)}} |f\rangle \langle f| \right) \quad (\text{S61k})$$

$$= \langle Z_L(-t) Z_i Z_L(-t) Z_i \rangle_{\{|f\rangle: f \in \mathcal{F}_L^{(o)}\}}. \quad (\text{S61l})$$

In lines labeled as Eqs. (S61b) and (S61e) we used the invariance of the density matrix $|\Lambda_d\rangle \langle \Lambda_d|$ under multiplication by U_t , U_t^\dagger and $Z_i Z_{\bar{i}}$ from either left or right (since $|\Lambda_d\rangle$ is the eigenstate of all these operators with eigenvalue +1). In lines labeled as Eqs. (S61f) and (S61j) we assumed that the “butterfly” cone of the operator $Z_L(t)$ has not yet reached subsystem $\bar{\mathcal{A}}$; thus the “butterfly” time t_B approximately corresponds to the time when $\langle Z_1 Z_{\bar{1}} \rangle$ correlator starts decaying [see Fig. 3(d)]. We also wrote schematically Tr as $\text{Tr}_{\mathcal{A}} \text{Tr}_{\bar{\mathcal{A}}}$, where only $\text{Tr}_{\bar{\mathcal{A}}}$ is a true partial trace in the sense that it produces a RDM, for clarity; the outer $\text{Tr}_{\mathcal{A}}$ is a full trace of the RDM defined on subsystem \mathcal{A} that produces a scalar. Finally, $\mathcal{F}_L^{(o)}$ is the set of Rydberg-blockaded bitstrings on the OBC chain of length L , and the last equation is infinite-temperature average over the corresponding ensemble.

The approximate ZZ OTOC discussed above can be made exact. By our construction in the main text, Fig. 2(b), state $|\Lambda_d\rangle$ is also an eigenstate of the decoupled Hamiltonian $\tilde{H}(G_{\mathcal{A}} \cup G_{\bar{\mathcal{A}}}) = \tilde{H}(G_{\mathcal{A}}) + \tilde{H}(G_{\bar{\mathcal{A}}})$, where $G_{\mathcal{A}}$ and $G_{\bar{\mathcal{A}}}$ are isomorphic OBC chain graphs with L vertices. Per Theorem 7, the same state preparation protocol as that discussed in the main text in context of the dangler system can be applied to a system consisting of two decoupled chains — i.e., a system evolving under the Hamiltonian $\tilde{H}(G_{\mathcal{A}} \cup G_{\bar{\mathcal{A}}})$ [see Figs. S1(a) and S1(b)]. Alternatively, if the experiment has the capability to decouple the subsystems \mathcal{A} and $\bar{\mathcal{A}}$ (e.g., by moving the two subsystems apart via optical tweezers) it may be possible switch from H_d to the decoupled Hamiltonian $\tilde{H}(G_{\mathcal{A}}) + \tilde{H}(G_{\bar{\mathcal{A}}})$ once the system

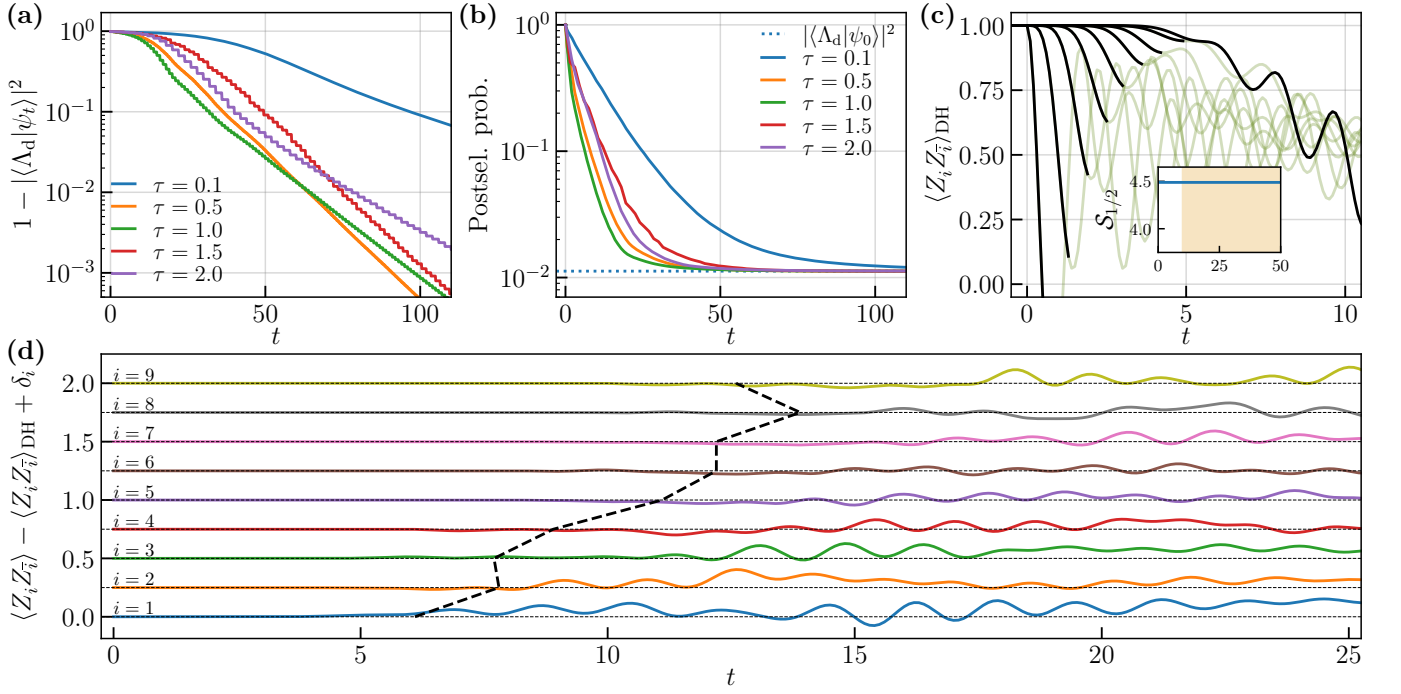


FIG. S1. Numerical study of an $N = 2L = 18$ decoupled OBC chains system. (a),(b) State preparation via $Z_1 Z_{\bar{1}}$ measurements in a setting identical to that described in Figs. 3(b) and 3(c) in the main text. Note that the overall state preparation dynamics here is very similar to the example given in the main text; in fact, the rate of infidelity decay (a) is slightly faster in the decoupled system than in the dangler. (c) Quench experiment identical to that given in Fig. 3(d) in the main text. Note that, as expected, no change in the half-system entanglement entropy occurs in this case (inset). The observables, however, as was anticipated in the discussion regarding the “butterfly” time t_B , are hardly distinguishable from those in the dangler system. (d) Comparison between the approximate $-\langle Z_i Z_{\bar{i}} \rangle$ and exact $-\langle Z_i Z_{\bar{i}} \rangle_{\text{DH}}$ OTOC proxies with shifts $\delta_i = (i - 1)/4$ added for clarity. The dotted line approximately marks off the range of validity of the “butterfly” time approximation for each i based on some heuristic detection of the onset of “significant” deviation between the two expectation values (the specifics of the heuristic are unimportant for this discussion).

is prepared in the eigenstate $|\Lambda_d\rangle$. In either case, the same quench protocol as discussed earlier will allow to measure the exact ZZ OTOC on the subsystem \mathcal{A} at any time t .

Since $[\tilde{H}(G_{\mathcal{A}}), \tilde{H}(G_{\bar{\mathcal{A}}})] = 0$, the unitary evolution operator decouples into commuting terms: $U_t = U_{\mathcal{A}} U_{\bar{\mathcal{A}}}$, where each term has support only on its corresponding subsystem and the time t is kept implicit. Then, following similar steps as before and simplifying, we have

$$\begin{aligned}
\langle Z_i Z_{\bar{i}} \rangle &= \text{Tr} \left(Z_i Z_{\bar{i}} U_{\bar{\mathcal{A}}}^\dagger U_{\mathcal{A}} Z_L U_{\mathcal{A}}^\dagger U_{\bar{\mathcal{A}}}^\dagger |\Lambda_d\rangle \langle \Lambda_d| U_{\bar{\mathcal{A}}} U_{\mathcal{A}} Z_L U_{\mathcal{A}}^\dagger U_{\bar{\mathcal{A}}}^\dagger \right) \\
&= \text{Tr} (Z_i Z_{\bar{i}} Z_L(-t)_{\mathcal{A}} |\Lambda_d\rangle \langle \Lambda_d| Z_L(-t)_{\bar{\mathcal{A}}}) \\
&= \text{Tr} (Z_i Z_{\bar{i}} Z_L(-t)_{\mathcal{A}} Z_i Z_{\bar{i}} |\Lambda_d\rangle \langle \Lambda_d| Z_L(-t)_{\bar{\mathcal{A}}}) \\
&= \text{Tr} (Z_L(-t)_{\mathcal{A}} Z_i Z_L(-t)_{\bar{\mathcal{A}}} Z_i |\Lambda_d\rangle \langle \Lambda_d|) \\
&= \langle Z_L(-t)_{\mathcal{A}} Z_i Z_L(-t)_{\bar{\mathcal{A}}} Z_i \rangle_{\{f\}:f \in \mathcal{F}_L^{(o)}\}},
\end{aligned} \tag{S62}$$

where $Z_L(-t)_{\mathcal{A}}$ is operator Z_L evolved under $\tilde{H}(G_{\mathcal{A}})$ in the Heisenberg picture. Since $\tilde{H}(G_{\mathcal{A}})$ doesn't have support on the subsystem $\bar{\mathcal{A}}$, $Z_L(-t)_{\mathcal{A}}$ never spreads outside of subsystem \mathcal{A} (meaning it commutes with any operator with support on subsystem $\bar{\mathcal{A}}$ only), and no approximations related to t_B are necessary. We show the exact OTOC measurements in Fig. S1(c) and compare them with the corresponding approximate measurement using the dangler Hamiltonian in Fig. S1(d). Note that while approximation in Eq. (S61f) is valid for times up to $(L + \bar{i})/v_B$ where v_B is the “butterfly” velocity, a more conservative estimate is assumed in Eq. (S61j); that being $t_B \sim L/v_B$ — which appears to be around $t_B \sim 5$ for the cases shown in Figs. 3(d) and S1(c) — since beyond this time $Z_L(-t)$ will be affected by the interaction term between the two half-systems of the dangler. Interestingly, this latter effect appears relatively smaller than expected, and for spins farther from the link connecting the two subsystems (i.e., from spins 1 and $\bar{1}$) the agreement between exact and approximate OTOCs in Fig. S1(d) holds for significantly longer than t_B .

As was mentioned in the main text, there is strong numerical evidence that the dimension of the simultaneous eigenspace of $\tilde{H}_{\text{PXP}}(G_C)$, where G_C is an arbitrary graph, and some $Z_i Z_{\bar{i}}$ on \mathcal{R} is typically exactly equal to the number of distinct $|\tilde{\Lambda}\rangle$ -type eigenstates whose pairing pattern contains pair (i, \bar{i}) . This means that the state preparation protocol discussed in the main text can be applied to an arbitrary system given that it hosts a $|\tilde{\Lambda}\rangle$ -type eigenstate with some known pairing pattern (see also Sec. VII). Although our analysis of the approximate and exact OTOCs was done in the context of the dangler and disconnected OBC chains, no specific assumptions related to these systems had been made, so the same analysis applies to generic systems that host $|\tilde{\Lambda}\rangle$ -type eigenstates. Therefore, having prepared such a system in the desired $|\tilde{\Lambda}\rangle$ -type state, one can execute the approximate or exact OTOC measurement protocol with essentially no difference from the two cases we addressed. For example, one could study operator spreading on a two-dimensional OBC lattice.

IX. STABILITY OF THE STATE PREPARATION AND OTOC PROTOCOLS TO PERTURBATIONS

Here we briefly investigate the effects of perturbations on the state preparation and quench protocols discussed in the main text and in Sec. VIII of this Supplemental Material. The intent of this section is to show that the dynamics involving $|\tilde{\Lambda}\rangle$ -type states has a degree of robustness to small perturbations, even if such perturbations prevent $|\tilde{\Lambda}\rangle$ from being an exact eigenstate of the full Hamiltonian. In this demonstration, we will perturb the dangler Hamiltonian $\tilde{H}_{\text{PXP}}(G_C)$ with

$$\delta H = \sum_{i \in V} \delta_i Z_i, \quad (\text{S63})$$

where V is the set of vertices of G_C , and the Zeeman fields δ_i are chosen randomly from a normal distribution with mean μ and variance σ^2 , $\delta_i \sim \mathcal{N}(\mu, \sigma^2)$. We find that the results are qualitatively similar for randomized and uniform ($\sigma = 0$) perturbations. The performance of the protocols gradually degrades as μ or σ get larger. In particular, in the numerical simulations presented in Figs. S2–S4 we set $\mu = 0$ and only varied σ with the goal of modeling some experimentally undesirable non-uniform zero-mean Zeeman field; in these simulations, for each value of σ , we used a single fixed random sample of the δ_i coefficients in Eq. (S63). (In a more careful analysis the averages would be calculated over many such samples, but our goal here is to demonstrate the qualitative behavior only.)

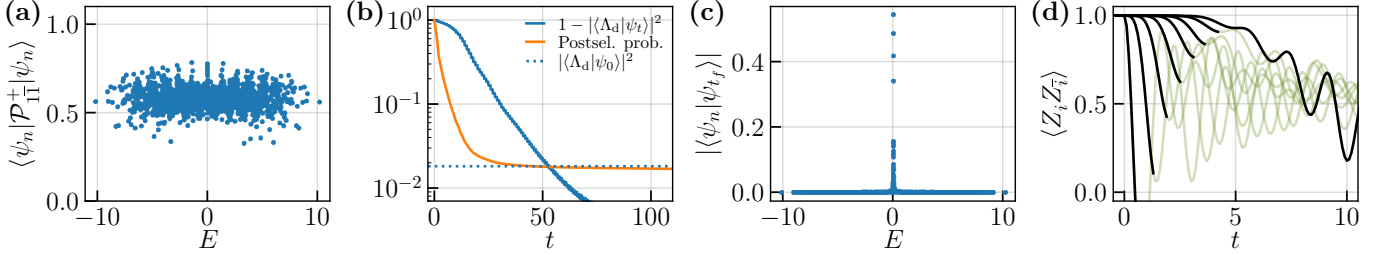


FIG. S2. Perturbed dynamics with $\sigma = 0.01$ on a dangler system of size $N = 2L = 16$. (a) Squared projections of eigenstates onto the +1 eigenspace of $Z_1 Z_{\bar{1}}$. Note that the perturbation destroys the degenerate nullspace of $\tilde{H}_{\text{PXP}}(G_C)$ as an eigenstate; there is no longer any simultaneous eigenstate of $\tilde{H}_{\text{PXP}}(G_C)$ and $Z_1 Z_{\bar{1}}$. (b) State preparation protocol with the interval between measurements $\tau = 1.0$. Since the system has no simultaneous eigenstates of the full Hamiltonian and $Z_1 Z_{\bar{1}}$, the postselection probability doesn't saturate like in the clean case but instead undergoes a very slow decay following its initial fast drop toward $|\langle \Lambda_d | \psi_0 \rangle|^2$ similar to that in the clean case. The infidelity of the postselected state with respect to $|\Lambda_d\rangle$ decays similarly to the clean case, but is expected to eventually saturate at some finite value. (c) Overlap of the state prepared via postselection on the +1 outcomes of $Z_1 Z_{\bar{1}}$ with the eigenstates of the full Hamiltonian. The protocol drives the system into a superposition of many eigenstates with energies close to zero. (d) Quench under the perturbed Hamiltonian from the initial state $Z_L |\psi_{i_f}\rangle$, where $|\psi_{i_f}\rangle$ is the actual state prepared by the postselection protocol in (b). The observables are essentially indistinguishable from the clean case.

Even though eigenstate $|\Lambda_d\rangle$ is destroyed by the perturbation, the simulations in Figs. S2–S4 clearly indicate that both the state preparation and quench dynamics retain most of the attributes found in the unperturbed case given the strength of the perturbation does not exceed some critical threshold [cf. Fig. S5]. A more careful analysis of this threshold and its scaling with system size in a realistic experimental setting will be left to another study.

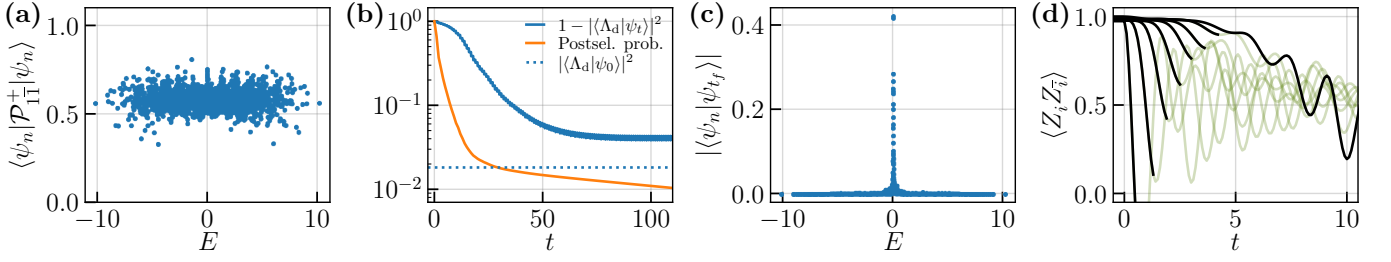


FIG. S3. Perturbed dynamics with $\sigma = 0.02$. (a)-(d) Same as in Fig. S2. Note that the decay of the postselection probability becomes more noticeable here than in the $\sigma = 0.01$ case [Fig. S2]. The infidelity of the postselected state with respect to $|\Lambda_d\rangle$ does not decay indefinitely like in the clean case, but saturates at a small finite value. This indicates a very large overlap of the postselected state with $|\Lambda_d\rangle$.

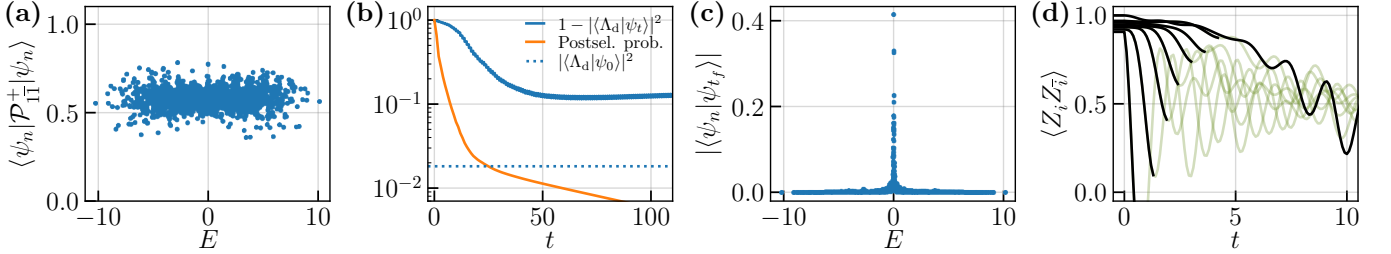


FIG. S4. Perturbed dynamics with $\sigma = 0.03$. (a)-(d) Same as in Figs. S2 and S3. Here the decay of the postselection probability is even steeper than in the previous two examples. Note, however, that the rate of decay of the postselection probability will depend on specific noise realization; i.e., it varies significantly depending on the random choices of the coefficients in Eq. (S63). This means that in an experiment there will be implicit postselection of “better” noise realizations, which also come with lower state infidelities. Here the effects of the perturbation on the OTOCs are already noticeable; however, the signal is still very close to that in the nearly unperturbed $\sigma = 0.01$ case.

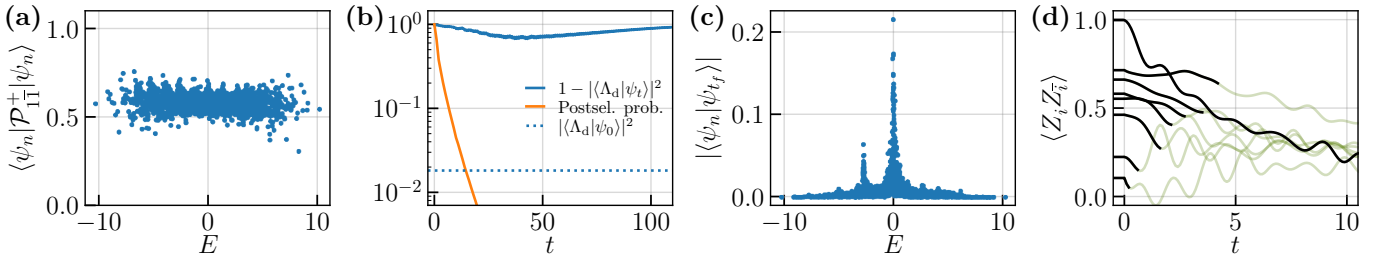


FIG. S5. Perturbed dynamics with $\sigma = 0.1$. (a)-(d) Same as in Figs. S2–S4. Strong perturbation breaks the state preparation protocol, but also drastically suppresses the postselection probability, which means situations like this are easily identifiable in experiments. As expected, the quench dynamics in (d) no longer closely resembles the clean case.

X. STATE PREPARATION PROTOCOL ENHANCEMENTS

Here we briefly explore possible enhancements to the state preparation protocol discussed in the main text. For concreteness, our examples will continue using the dangler geometry with $N = 2L$ spins; however, everything will apply to other systems hosting $|\Lambda\rangle$ -type eigenstates.

In general, the total number of measurements and time needed to prepare the system in the target state $|\Lambda_d\rangle$ with high fidelity can be reduced via a combination of two strategies: (1) increasing the overlap of the initial state with $|\Lambda_d\rangle$, and (2) performing measurements of more than a single pair of spins.

For an illustration of the first strategy, suppose it is possible to prepare Bell pairs

$$|\Phi^-\rangle = \frac{1}{\sqrt{2}} (|00\rangle - |11\rangle). \quad (\text{S64})$$

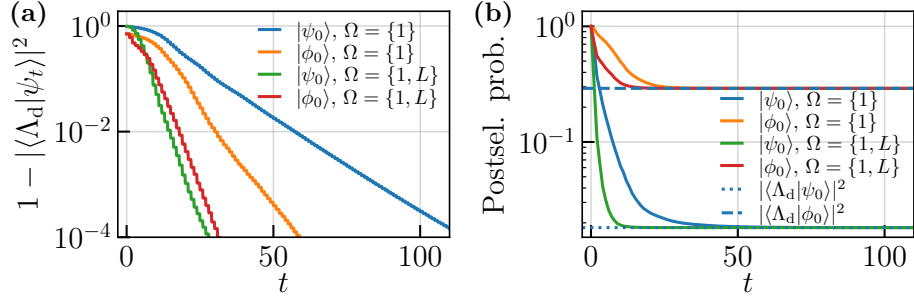


FIG. S6. Dependence of the infidelity (a) and postselection probability (b) on the choice of the initial state and number of simultaneously measured spin pairs in an $N = 2L = 16$ dangler system with the interval between measurements $\tau = 1.0$. Here $|\psi_0\rangle = |00 \dots 0\rangle$, $|\phi_0\rangle$ is the state in Eq. (S65), and the composite evolution and projective measurement operator is given by Eq. (S67) with the sets Ω as specified in the legend.

Then, assuming L is even, consider state

$$|\phi_0\rangle = \bigotimes_{i=1}^{L/2} \left(|\Phi^-\rangle_{2i-1, 2i} |00\rangle_{2i, 2i} \right), \quad (\text{S65})$$

which can be prepared via two-qubit gates without violating the Rydberg blockade. Its overlap with $|\Lambda_d\rangle$ is

$$\langle \phi_0 | \Lambda_d \rangle = \sqrt{\frac{2^{L/2}}{F_{L+2}}} = 2^{L/4} \langle \psi_0 | \Lambda_d \rangle, \quad (\text{S66})$$

where $|\psi_0\rangle = |00 \dots 0\rangle$ is the initial state used in the main text. This is already a significant enhancement, strongly suppressing the exponential decay with L [comparing $F_{L+2} = C\phi^L \approx C(1.618)^L$ vs $F_{L+2}/2^{L/2} = C(\phi/\sqrt{2})^L \approx C(1.144)^L$]. Note that in an actual experiment one may be able to produce initial states that have even greater overlaps with $|\Lambda_d\rangle$ by entangling all pairs of spins (as opposed to only half of them as in $|\phi_0\rangle$) and relying on the natural Rydberg blockade.

As for the second strategy, consider postselection on the +1 outcomes of a set of independent and simultaneous projective measurements $\mathcal{P}_{ii}^+ = |00\rangle\langle 00|_{ii} + |11\rangle\langle 11|_{ii}$, $i \in \Omega$, where $\Omega \subseteq \{1, \dots, L\}$. This corresponds to the following generalized composite evolution and projective measurement operator M'_τ :

$$M'_\tau = \left(\prod_{i \in \Omega} \mathcal{P}_{ii}^+ \right) e^{-iH_d \tau}. \quad (\text{S67})$$

Setting $\Omega = \{1\}$ reduces M'_τ to M_τ in the main text, whereas setting Ω to any other non-empty subset of $\{1, \dots, L\}$ results in an extended and generally more efficient operator that is also somewhat less sensitive to the speed of information scrambling in the system (i.e., the optimal frequency of measurements typically increases if one adds additional spin pairs to the protocol).

The two strategies discussed above are demonstrated in Fig. S6. Note that while the second strategy reduces the number of measurements needed for preparing the target state with desired fidelity, it cannot increase the overall postselection probability, which depends solely on the overlap of the initial state with $|\Lambda_d\rangle$.